Collective motion of a finite sized Vicsek flock: I know why the caged bird flocks

THESIS

submitted in partial fulfillment of the
requirements for the degree of

MASTER OF SCIENCE
in
PHYSICS

Author : Leandros Talman

Student ID :

Supervisor : Luca Giomi

2^{nd} corrector : Helmut Schiessel

Leiden, The Netherlands, May 31, 2017

Collective motion of a finite sized Vicsek flock: I know why the caged bird flocks

Leandros Talman

Instituut-Lorentz, Leiden University
P.O. Box 9500, 2300 RA Leiden, The Netherlands

May 31, 2017

Abstract

The Vicsek model offers a phenomonologically rich set of behaviours while maintaining simple rules of interaction. By introducing a convex hull as a means of providing cohesion within the system, we have been able to probe the behaviour of this model as it is moved off of the usual periodic boundary conditions, to the infinite plane. We present the findings of 4 different schemes that introduce this cohesive effect by way of deflecting Boids on the convex hull back into the bulk. In one such scheme, a new phase transition is found, between a state wherein the flock has a constant direction of motion, and a state where this direction precesses. The rate of precession is found to be dependent on both the noise level and the deflection coupling.

Contents

1 Introduction **1**
1.1 Swarming 1
1.2 Boids and the Vicsek model 4
1.2.1 Continuum treatment: Toner and Tu 7
1.3 Changes to the Vicsek model 11
1.4 Moving the Vicsek model to the infinite plane 13
1.4.1 Convex Hull Force Recipes 13
1.4.2 Observables 17

2 The simulation **23**
2.1 The program 23
2.1.1 Interaction algorithms 24
2.1.2 Updating positions 29
2.1.3 Finding the new convex hull 30

3 Results **33**
3.1 Local Curvature 34
3.1.1 Ordered regime 34
3.1.2 Disordered regime 42
3.1.3 Conclusion 46
3.2 Flock Mean 48
3.2.1 Ordered regime 48
3.2.2 Disordered regime 53
3.2.3 Conclusion 55
3.3 Near Neighbour 56
3.4 Far Neighbour 57

Version of May 31, 2017– Created May 31, 2017 - 17:35

Chapter 1

Introduction

1.1 Swarming

Flocking, herding, schooling or, more generally, swarming, is the collective behaviour of groups of animal groups. It has long been studied by biologists in a multitude of environments and with a wide array of organisms.
On and above the human length scale, a large variety of subjects exhibiting this behaviour can be found, e.g. bird flocks, fish schools, land animal herd behaviour, and even large masses of humans. However, the same phenomenon is known to occur on scales far smaller than our own, such as in bacterial colonies and even within the cells of organisms: a well-known *in-vivo* example of this is the assembly of a cytoskeletal framework by means of microtubules, a lattice of tubulin dimers that is responsible for maintaining the structural integrity and coordinating the division of cells. In the field of active matter, these microtubules, when mixed with motor proteins such as kinesin, form an oft-used medium of liquid crystals that display interesting topological features, e.g. nematic, smectic or chiral ordering, due to their ability to convert the chemical energy from a substrate (such as a solution of ATP) into sliding movement. The elongated nature of these microtubules, coupled with the longitudinal motion caused by kinesin motor proteins stuck to these tubules, causes them to flow and fold. At the same time, topological features such as defects are kept intact, as the 2D surface they are kept on forces tubules to align locally.
Whatever the length scale may be, swarming behaviour (henceforth in this thesis referred to as "flocking") typically occurs in groups of agents ("flocks") that comprise a volume orders of magnitude larger than the volume of a single agent ("boid").

Figure 1.1: *Some examples of flocking behaviour with systems of length scales larger than humans.* **Top left***: A school of Bigeye scad near Hawaii form schools to minimise their chance of being caught by predators. The size of the "baitball" can exceed that of a typical house, containing hundreds of thousands of individuals.* **Top right***: A murmuration, or flock of starlings. Like the Bigeye Scad, these birds band together to ward off their chances of being struck by a nearby predator, such as a falcon. These flocks can contain on the order of a tens of thousands of individuals, taking up volumes in the tens of thousands of cubic meters.* **Bottom left***: A stampeding herd of African Buffalo. Stampedes are typically instigated by the perception of danger by few individuals. This information travels through the herd at a speed much greater than the animals themselves and causes a quick alignment. Such herds can contain on the order of hundreds of thousands of individuals and span multiple square kilometers.* **Bottom right***: A highly ordered flock of humans forming a military parade. In this case, not only is directional alignment important, but also position, gait, posture and the positions of all limbs are expected to be roughly the same in the entire flock.*

From a physicist's perspective, this presents an interesting phenomenon: how can such long-range orientational order arise so far from equilibrium, when objects as simple and small as molecules can exhibit it? In most cases, it is impossible for a boid to sense the behaviour of the flock as a whole: a buffalo on one end of a 100,000-strong herd will be hard-pressed to account for the movement of all other buffalo, if it was even able to observe them all. Furthermore, there is no indication that there is some sort of central director "calling the shots" and orienting all boids, such as

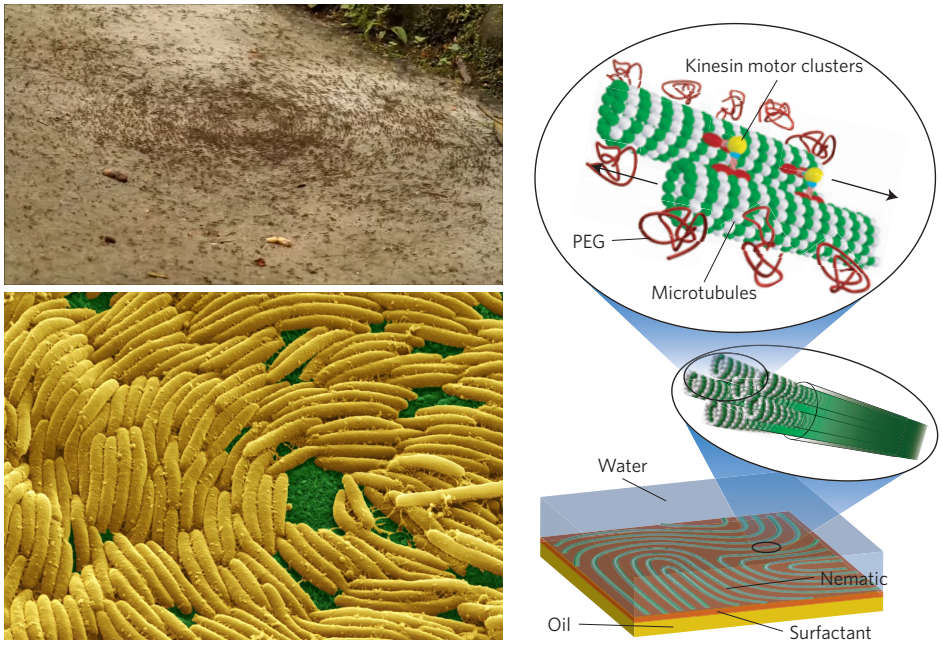

Figure 1.2: *Some examples of flocking behaviour with systems on length scales smaller than humans.* **Top left***: An "ant mill." This phenomenon happens in certain species of ants whose primary mode of sensing is through smell rather than sight. If the pheromones they follow dilute too much, they may start following one another in a circular manner, sometimes until dying of exhaustion.* **Bottom left***:* Myxococcus Xanthus*, a Gram-negative rod bacterium that starts to behave in a cooperative fashion when nearing starvation.* **Right***: A schematic of how microtubules are used as a basis for an experiment in active nematics. The kinesin motor proteins cause the different microtubules to slide along one another whereby the elongated nature of the microtubules forces alignment in the 2D plane they are kept in. From [1]*

a central computer as used for research in cooperative drone behaviour. As such, it seems reasonable to assume that, barring the possibility of the boids sensing some quantity that is directly related to the behaviour of the flock as a whole, each boid will instead make a "first-order" estimate, observing the behaviour of its direct neighbours by way of sight, sound, haptic or chemical senses.

The ubiquity of this phenomenon raises some interesting questions:

- How complex can the "rules of interaction" between agents be, if this phenomenon is to be found in entities as simple as microtubules?
- How robust is this behaviour if we perturb or drive the system in a certain manner, and what is the nature of the change in behaviour

when perturbed?

- Is there a limit to the size of these flocks, i.e., how does the cooperation correlate in space?

A great effort has been made to answer these questions, both experimentally and theoretically, with simulations and analytical work to explain the phenomena found. These include empirical measurements in natural (e.g. starling flocks [2], fish schools[3] and herds of zebra [4]), and laboratory (bacterial colonies[5], migrating tissue cells [6] and army ants [7]) environments. As these all involve complex agents, better controlled experiments, attempting to boil these questions down to elementary problems have been done by:

- Placing thousands of apolar rods (made of brass or simply rice grains) on a bowl, and then vibrating the bowl[8]. To lower the energy of the system, rods must align locally to minimise the empty space and amount of overlap in the xy-plane. This in turn may cause the formation of topological defects.

- Creating a 2D interface of water and oil, on which a solution of ATP, microtubules and kinesin motor proteins is located (see Fig. 1.2 right). The kinesin attaches to the microtubules and, burning ATP, causes them to slide along eachother. Due to the elongated nature of the tubules and the fact that they stay on the interface, they tend to align locally. On large scales, they too can form topological defects.

1.2 Boids and the Vicsek model

One of the first steps toward simulating collective motion, "Boids" (hence our use of the term), was made by Reynolds[9], implementing rules that allow for repulsion, attraction and alignment. It has since found use in the coordination of physical swarms such as large numbers of areal and terrestrial drones. However, the program was not made for measurement, but for the creation of realistic behaviour in computer graphics, and to this end it has seen use in some video games and feature films in the 1990s.
The first step toward a quantitative simulation was done in 1995, when Tamás Vicsek et al. published *Novel type of phase transition in a system of self-driven particles*[10]. In it, they introduced a minimal model (now referred to as the "Vicsek model") of flocking, based on a simple rule of alignment: each boid, initially placed randomly to achieve a desired number density ρ, moves with constant speed v_0 in a certain, initially random,

direction θ_b^0 on a periodic boundary system with volume $V = \frac{N}{\rho}$. Each timestep, the boids synchronously update their direction according to the average direction of agents within a radius r_0 of itself, plus an error term. In mathematical terms,

$$\begin{aligned}\theta_b^{t+1} &= \left\langle \theta_{b'}^t \right\rangle_{r_0} + \eta\xi_b^{t+1} = \operatorname{atan}\left(\frac{\left\langle v_y \right\rangle_{r_0}}{\left\langle v_x \right\rangle_{r_0}}\right) + \eta\xi_b^{t+1} \\ &= \operatorname{atan}\left(\frac{\left(\sum_{<b,b'>} \mathbf{v}_{b'}\right)_y}{\left(\sum_{<b,b'>} \mathbf{v}_{b'}\right)_x}\right) + \eta\xi_b^{t+1}\end{aligned} \tag{1.1}$$

where the subscript r_0 and the sum over $< b, b' >$ both indicate that only those boids b' whose distance $d_{b,b'} = |\mathbf{r}_{b,b'}| = |\mathbf{r}_b - \mathbf{r}_{b'}|$ to boid b are equal to or below r_0. The error term $\xi_b^{t+1} \in \mathcal{U}(-\pi, \pi)$ is a white noise distributed number with neither spatial nor temporal memory. The position is then updated according to

$$\mathbf{r}_b^{t+1} = \mathbf{r}_b^t + v_0\hat{\mathbf{n}}\left(\theta_b^{t+1}\right) \tag{1.2}$$

Where $\hat{\mathbf{n}}(\theta) = \left(\cos\theta\hat{\mathbf{i}} + \sin\theta\hat{\mathbf{j}}\right)$ is a unit vector in direction θ. To differentiate states wherein the system was organised and disorganised, Vicsek et al. introduced an order parameter

$$P_T = |\mathbf{P}_T| = |\langle \mathbf{v}_b \rangle| = \frac{1}{N}\left|\sum_b \mathbf{v}_b\right|, \tag{1.3}$$

which goes to zero for disorder and approaches 1 for full order. We will use the same parameter, but we will call it the total polarisation parameter P_T for reasons that will become apparent later.

The Vicsek model is similar to the XY model, a $U(1)$ rotationally symmetric version of the Ising model, which is a staple of statistical mechanics. It differs from this in that it is off-lattice, and the objects move. Indeed, if we were to set the speed to zero, it would reduce to an off-lattice XY model, with behaviour dependent on the noise level of the boids, as well as the density: a percolation threshold of $\rho = 1$ exists, below which no ordered behaviour would be exhibited.

The Vicsek model displays different behaviour for different parameters: for very low density ($\rho \ll 1$), small noise levels can induce disorder, similar to a percolation threshold: if boids are to rarely encounter neighbours, their trajectories will devolve into random walks. For high density, there

is a much larger range of noise levels before boids no longer move collectively. Still, there is always a transition from high order to low order, when the noise levels are raised beyond a certain critical noise value $\eta_C(\rho)$.
In their 1995 paper, Vicsek et al. concluded the transition to be of second order, motivated by a smooth decrease in the order parameter (See Fig. 1.3) as function of noise. even when increasing the number of boids in the system, which seemed to converge the steepness to a certain infinite system value. Consequently, they calculated critical exponents for both the density and noise which were not reproduced by others.

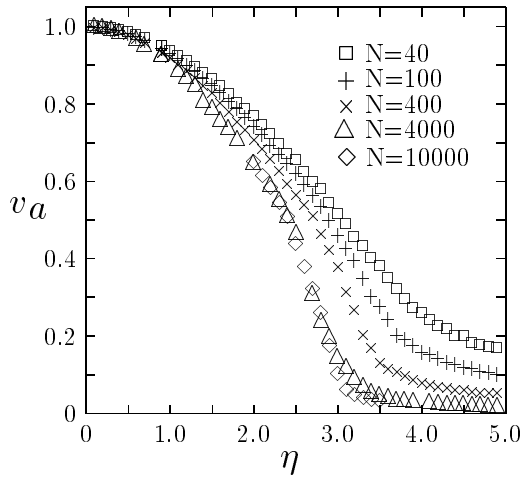

Figure 1.3: *Order parameter P_T (Vicsek et al. called it v_a) as function of noise level η (multiplied by 2π compared to our definition)*

The nature of the transition was later contested by Grégoire et al. in [11], who claimed that the transition is of first order in all cases of local alignment, in 2D. Only in 2015 was this matter settled, with the publication of [12] by Solon et al., where it was found that there is a coexistence phase consisting of one or multiple high-density ordered bands (2D) or sheets (3D) of boids, all moving in the same direction, with low-density disordered voids inbetween. Consequently, they found the following phase diagram:

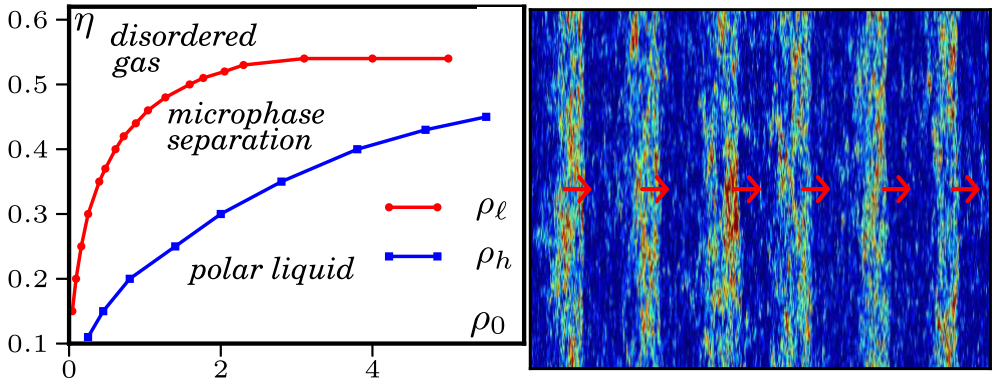

Figure 1.4: ***Left:*** *Phase diagram of the Vicsek model. Between the states of full order (polar liquid) and full disorder (disordered gas, though there is no distribution of speeds as all Boids move at the same speed), a region of phase space exists where the system is divided into sections that are highly polarised and sections that are not: a microphase state.* ***Right:*** *Snapshot of the microphase state. A number of high density ordered bands (coloured green), moving parallel to one another, move through the lower density system (blue). They are locally highly ordered, while the "void" between is not. Proportional to the initial density, the number of bands increases until the system contains enough bands such that the entire system is ordered.*

In between the regions of disorder ($P_T \to 0$) and order ($P_T \to 1$, up to some error, dependent on η and N) lies a regime of microphase separation. This microphase separation allows for the existence of highly polarised ordered bands traveling in the same direction, where the number density of Boids is greater than in the unpolarised "voids" between these bands. As the initial density is increased, the number of bands increases, until finally, the system is entirely polarised. These polarised bands lead to so-called Giant Density Fluctuations (GDF), where the notion of density is no longer well-defined: normally a region of volume V having on average N particles enclosed would display density fluctuations with standard deviation ΔN proportional to $\sqrt{N}$. Thus, increasing the volume measured in would decrease these fluctuations as $1/\sqrt{V}$. In these strongly polarised phases of active matter, however, Toner and Tu predicted these fluctuations to grow faster than $\sqrt{N}$, in some cases as fast as N (See [13] and [14]).

1.2.1 Continuum treatment: Toner and Tu

The fact that long-range orientational order could arise at all in the 2D version of the Vicsek model was in itself a surprise, as it seems to violate the Mermin-Wagner theorem, which states that no continuous symmetry (the

Version of May 31, 2017– Created May 31, 2017 - 17:35

polarisation direction) can be broken spontaneously at a finite temperature (noise level) in systems with short-range interactions. We will first briefly give a rough explanation of the motivation for this intuition, and then show why it is not the case.
Let us first take the difference in direction between consecutive timesteps for a single boid:

$$\begin{aligned} \theta_b^{t+1} &= \left\langle \theta_{b'}^t \right\rangle_{r_0} + \eta \xi_b^{t+1} \\ \theta_b^{t+1} - \theta_b^t &= \left\langle \theta_{b'}^t \right\rangle_{r_0} - \theta_b^t + \eta \xi_b^{t+1} \end{aligned} \tag{1.4}$$

Now, we rewrite some terms on both sides by coarse graining, i.e. we look at behaviour on length and time scales far larger than microscopic interactions. The lhs becomes the partial derivative with respect to time:

$$\theta_b^{t+1} - \theta_b^t \to \theta\left(\mathbf{r}, t+dt\right) - \theta\left(\mathbf{r}, t\right) = \partial_t \theta\left(\mathbf{r}, t\right) \tag{1.5}$$

while the rhs resembles the discrete version of the Laplacian:

$$\left\langle \theta_{b'}^t \right\rangle_{r_0} - \theta_b^t = \frac{1}{N} \sum_{\langle b,b' \rangle} \left(\theta_{b'}^t - \theta_b^t\right) + \eta \xi_b^{t+1} \tag{1.6}$$

$$= D \nabla^2 \theta_b^t + \eta \xi_b^{t+1} \tag{1.7}$$

To see this, consider having a lattice of 4 boids surrounding boid b:

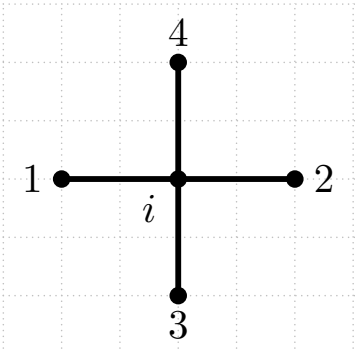

Then

$$\begin{aligned} \left(\theta_1^t - \theta_b^t\right) &= -\partial_x \theta_1^t \\ \left(\theta_2^t - \theta_b^t\right) &= \partial_x \theta_b^t \end{aligned} \tag{1.8}$$

and

$$\partial_x \theta_b^t - \partial_x \theta_1^t = \partial_x \left(\partial_x \theta_b^t\right) \tag{1.9}$$

The same happens for boids 3 and 4 in the $y-$direction, and so we recover the Laplacian

$$\partial_x \left(\partial_x \theta_b\right) + \partial_y \left(\partial_y \theta_b\right) \tag{1.10}$$

So now we have

$$\partial_t \theta = D\nabla^2 \theta + \eta\xi \tag{1.11}$$

which describes a noisy diffusion. Thus, if we now let a single boid make a departure θ_0 from the flock average at $t = 0$, this offset spreads through the rest of the system by diffusion, and so the mean-square spread of this error will scale as $\sqrt{t}$.
This error is also conserved: the sum of all offsets induced by this single error must equal θ_0:

$$\partial_t \int \theta d^d r = D \int \nabla^2 \theta d^d r = D \int \nabla\theta \cdot d\mathbf{S} \tag{1.12}$$

Which is zero when the flock size is much larger than $\sqrt{t}$.
At a time t, then, all boids within this area will have been given an offset

$$\theta\left(t\right) \approx \frac{\theta_0}{N} \approx \frac{\theta_0}{t^{d/2}} \tag{1.13}$$

For all $d > 2$, this decays sufficiently such that long-range order can arise, purely due to the fact that the error is spread out quickly to enough neighbours such that this new direction will be assumed by the flock.
This analysis only applies to a single error, however. In reality, errors are being made by all boids at each timestep. In order for the errors to propagate to the arbitrarily large total system size r, a time $t_D\left(r\right) \propto r^2$ is required to pass. During this time, each boid makes t_D errors. Assuming a homogeneous and isotropic system, the number of boids scales as the volume, r^d, and so the total number of errors is proportional to $r^d t_D = r^{d+2}$. Then the RMS error per boid $\delta\theta$ is proportional to $r^{1-d/2}$. For $d \leq 2$, if we take $r \to \infty$, this value becomes arbitrarily large, and so no long-range order should be possible.
The reason for this apparent violation was given by Toner and Tu in [13], where they explained that distinction lies in the fact that the boids initially move already: The Mermin-Wagner theorem applies to equilibrium systems, which the Vicsek model decidedly is not. Due to the fact that the motion is implied in the model, the propagation of errors is not isotropic: in the direction of motion, the effect of errors is smaller than in the transverse direction, i.e. the departure from the original transverse position is

proportional to the RMS error in the transverse speed, which is proportional to the RMS error in the direction:

$$\delta x_\perp \propto \delta v_\perp t \propto v_0 \delta\theta t \tag{1.14}$$

As $\delta\theta \propto r^{1-d/2} \propto t^{1/2-d/4}$, $\delta x_\perp \propto t^{3/2-d/4}$. In the transverse direction, the error has propagated to a width $t^{1/2}$, and so in fact the actual spatial deviation of a boid, caused by its error, will overtake the speed at which the error diffuses. This means that, in $d < 4$, it is the transport of the boid itself that influences other, initially far-off boids, rather than a passing on of the error. This thus means that the volume of the region to which errors have spread in a time t, is given by the product of the lateral direction in which it has spread diffusively, $\sqrt{t}$, and the transverse width in which the boid has moved, $w_\perp(t)$. In this region, again the total number of errors made is proportional to the volume and t. It thus grows as sufficiently so that in $d < 4$, rather than diffusion dominating the change in direction, it is in fact the transverse motion itself that propagates errors. Now, if we look at the volume of a region affected by the error of a boid, it is given by a diffusive length $\sim \sqrt{t}$ in the direction of motion, and a width $w_\perp(t)$. The number of errors made in this region is again given by the product of the volume of this region and the time it has taken to become this size: $w_\perp(t)\, t^{3/2}$. Then the RMS error per boid should be given again by the square root of the number of errors, divided by the amount of boids: $\delta\theta \propto \frac{\sqrt{w_\perp(t) t^{3/2}}}{w_\perp(t)\sqrt{t}} \propto \frac{t^{1/4}}{w_\perp(t)^{1/2}}$. Now we already know that $w_\perp(t) \propto v_0\delta\theta t \propto \frac{t^{5/4}}{w_\perp^{1/2}}$ and so $w_\perp(t) \propto t^{5/6}$, much faster than the $\sqrt{t}$ of pure diffusion. Finally, we can plug this dependency of $w_\perp(t)$ on t back in the equation for $\delta\theta$ and see that

$$\delta\theta \propto \frac{t^{1/4}}{t^{5/12}} \propto t^{-1/6} \tag{1.15}$$

Which clearly goes to zero as $t \to \infty$. Thus true long range order indeed is possible. Before finding this argument, Toner and Tu also introduced hydrodynamic equations[14] for flocking by giving it a continuum treatment.

They are given by

$$\frac{\partial \rho}{\partial t} + \nabla \cdot (\mathbf{v}\rho) = 0, \tag{1.16}$$

$$\begin{aligned}&\partial_t \mathbf{v} + \lambda_1 (\mathbf{v} \cdot \nabla) \mathbf{v} + \lambda_2 (\nabla \cdot \mathbf{v}) \mathbf{v} + \lambda_3 \nabla \left(|\mathbf{v}|^2 \right) \\ &= \alpha \mathbf{v} - \beta |\mathbf{v}|^2 \mathbf{v} - \nabla P + D_B \nabla (\nabla \cdot \mathbf{v}) + D_T \nabla^2 \mathbf{v} + D_2 (\mathbf{v} \cdot \nabla)^2 \mathbf{v} + \mathbf{f}\end{aligned} \tag{1.17}$$

$$P = P(\rho) = \sum_{n=1}^{\infty} \sigma_n (\rho - \rho_0)^n \tag{1.18}$$

Where $\rho(\mathbf{r})$ is the density local boid density, $\mathbf{v}(\mathbf{r})$ is the velocity field (the first equation simply enforces the conservation of bird numbers), and $P(\rho)$ is a pressure that aims to maintain the number density at a mean value ρ_0. β, D_B, D_2 and D_T are positive constants and $\alpha < 0$ in the disordered phase and $\alpha > 0$ in the ordered phase. The different λ constants are comparable to those used in the Navier-Stokes equation. As this model does not have Galilean invariance (all boids move at the same speed and so not all frames of reference are equal), λ_2 and λ_3 are not zero, as is the case in the Navier-Stokes equation, and λ_1 is not equal to 1. Their values are instead set by the microscopic rules. The α and β terms cause the velocity field $\mathbf{v}(\mathbf{r})$ to have a finite magnitude $|\mathbf{v}(\mathbf{r})| = \sqrt{\frac{\alpha}{\beta}}$. D_L, D_1 and D_2 are diffusion constants that can be seen as viscosities (i.e. cause local alignment), which allow the fluctuations of the velocity field to spread out. Finally, $\mathbf{f}$ is a driving force that simulates the noise, i.e. the errors that boids make when picking a new direction. As mentioned before, it is a white noise with neither spatial nor temporal memory.

1.3 Changes to the Vicsek model

Being a minimal model of flocking, the Vicsek model has been modified copious times to introduce more complex phenomena that have been observed in nature, e.g. by reintroducing the attractive and repulsive components that were originally included in the Boids program [15], or a more realistic interaction that includes the limited eyesight of organisms [16]. While delivering quantitatively different results, the main properties of a phase transition and its order remain. In 2004, Grégoire et al. published results of a variant of the Vicsek model, where the implementation of noise was given by way of adding a random vector with length proportional to

the amount of neighbours, rather than a random term added to the direction:

$$\mathbf{v}_b^{t+1} = \mathcal{N}\left[\sum_{<b,b'>} \mathbf{v}_{b'} + n_B \eta \hat{\mathbf{n}}\left(\xi_b^{t+1}\right)\right] \tag{1.19}$$

with $\mathcal{N}[\mathbf{u}] = \frac{\mathbf{u}}{|\mathbf{u}|}$ a normalisation operator and n_B the number of boids within the interaction radius. A priori, this seems to disproportionately distort the direction of boids in high density sections of the flock, and this indeed was the intention: rather than assuming boids make the same mistake, regardless of the amount of neighbours (i.e. after having measured the average direction), they instead assume that an error is made with each measurement of the neighbours' directions. As mentioned in the previous section, the nature of the phase transition was contested by Grégoire et al. They reported on a different behaviour of the polarisation while using this form of noise, henceforth called "vectorial" noise, as opposed to the "scalar" noise of the original model, as seen in 1.5.

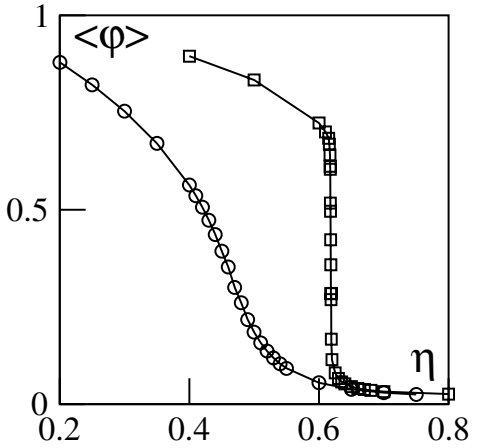

Figure 1.5: *Behaviour of the polarisation P_T (called ϕ in [11]) as function of the noise level η using $L = 32$ and $\rho = 2$ in both simulations: circles for scalar noise, squares for vectorial noise. As N increases, the sharpness of the scalar noise transition also increases. This requires systems of $N = 10^5$ boids and more to become apparent.*

Compared to the scalar noise implementation, the vectorial noise more accurately describes this transition while using far fewer numbers of boids. For this reason, we opted to use the vectorial noise in our simulations, as it allowed us to greatly speed up the computations and thus perform measurements on more combinations of parameters.

1.4 Moving the Vicsek model to the infinite plane

In *Linear Response to Leadership*[17], Pearce and Giomi introduced "leadership" to the Vicsek model. A subset of N_l boids is then given a constant offset ϕ_l to the updated θ_b^{t+1}, resulting in a precession of the polarisation vector at a rate proportional to $\tau = N_l \phi_l$. To measure this precession, they introduced a "curvature" observable:

$$\kappa(t) = \hat{z} \cdot (\mathcal{N}[\mathbf{P}(t-1)] \times \mathcal{N}[\mathbf{P}(t)]) \tag{1.20}$$

$$= \sin\left(\theta_{\mathbf{P}}^{t} - \theta_{\mathbf{P}}^{t-1}\right) \approx \theta_{\mathbf{P}}^{t} - \theta_{\mathbf{P}}^{t-1} \tag{1.21}$$

with the approximation holding due to the fact that the observed precession is small (on the order of 10^{-3}). In analysing this model's changes to the Toner-Tu equations, they came across an integral of the form $\int dA \nabla \cdot \mathbf{\Sigma}$, where $\mathbf{\Sigma}$ is an effective stress tensor that distorts the polarisation of the flock. As this integral must be zero by the divergence theorem on a periodic boundary, these stresses cancel out, with the dynamics of the total polarisation being purely diffusive when $\tau = 0$.
To probe the contribution of this term to the model, we opted to move the model to a system with no periodic boundaries, i.e. on an infinite plane. As the Vicsek model does not contain any mechanisms to preserve the number density of boids, we introduced various methods that caused boids to stay together. These are given in the next section. In the end, the behaviour we found with some of these methods was interesting enough that we actually dispensed with performing simulations involving leadership, and instead focussed only on the phenomena fed by moving the model to the infinite plane.

1.4.1 Convex Hull Force Recipes

In the infinite plane, any collection of boids under the subject of noise is going to diffuse until becoming sufficiently separated as to never interact again. In order to combat this, we introduced some cohesive components which we call force recipes. These forces act only upon those boids that make up the convex hull of the group, i.e. that convex set of boids that contains all boids within it. It can be seen as the set of boids at which a rubber band, released around the entire flock, would be attached to and make a corner: See Fig. 1.6. Finding this set of points can be done in a variety of ways, some more involved than others. We found an algorithm that strikes a balance between simplicity and computational speed called

"Monotone chain" or "Andrew's algorithm" In Chapter 2, we give a pseudocode version of this algorithm.

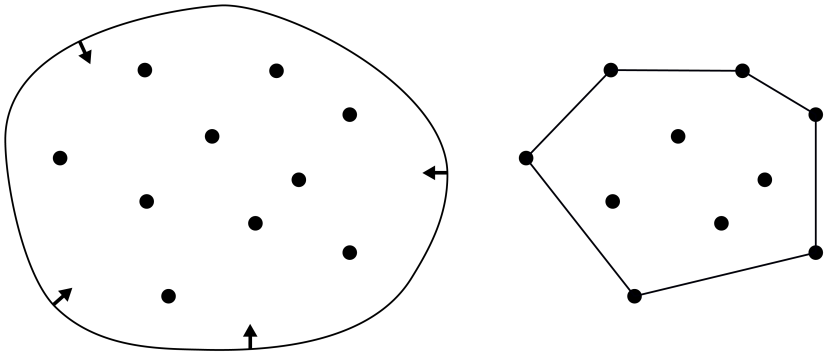

Figure 1.6: *The convex hull visualised by the rubber band analogy. If we were to release a rubber band (with equilibrium length smaller than the length of the convex hull), the convex hull would consitute those points at which the rubber band makes a turn.*

After calculating the force, it is applied by altering the direction of the boid, prior to moving it in that new direction:

$$\mathbf{v}_b^{t+1} = \mathcal{N}\left[\mathcal{N}\left[\sum_{<b,b'>} \mathbf{v}_{b'} + n_B \eta \hat{\mathbf{n}}\left(\xi_b^{t+1}\right)\right] + \gamma \mathbf{f}_b^{t+1}\right] \tag{1.22}$$

Rather than including the force within the first normalisation operator, the new direction based on neighbours and noise is first normalised before being updated with the force. This was done to make the influence of the convex hull independent of local boid density in the bulk. We decided on 4 different implementations of keeping boids within range of one another, each with its own motivation, which we will expand on below per recipe. From now on, we will omit the time-index for clarity.

Local Curvature

In the local curvature force recipe, we implement a discrete analogue of the surface tension of, for instance, a droplet of water. This surface tension is minimised when the curvature of the droplet is minimised. Thus, we point the force on a boid on the hull inward by taking the average normalised direction of neighbouring boids on the hull, and make it proportional to

the local curvature:

$$\mathbf{f}_h \equiv \kappa_h \mathbf{n}_h = \frac{d\mathbf{t}_h}{ds_h} \tag{1.23}$$

$$= \frac{1}{\frac{|\mathbf{t}_{h+1}|+|\mathbf{t}_h|}{2}} \left(\hat{t}_{h+1} - \hat{t}_h\right) = 2\frac{\hat{t}_{h+1} - \hat{t}_h}{|\mathbf{t}_{h+1}| + |\mathbf{t}_h|} \tag{1.24}$$

Where $h \in H$ is an index pointing to a boid on the hull. This list of indices is ordered counter-clockwise with respect to the position on the hull and so $h+1$ for the final value of h refers to the start of the list. $\mathbf{t}_h$ is the tangential vector of the convex hull pointing at boid h, i.e. the difference vector of the position of boid h and the position of boid $h-1$, and $\hat{t}_h$ is its normalised version.

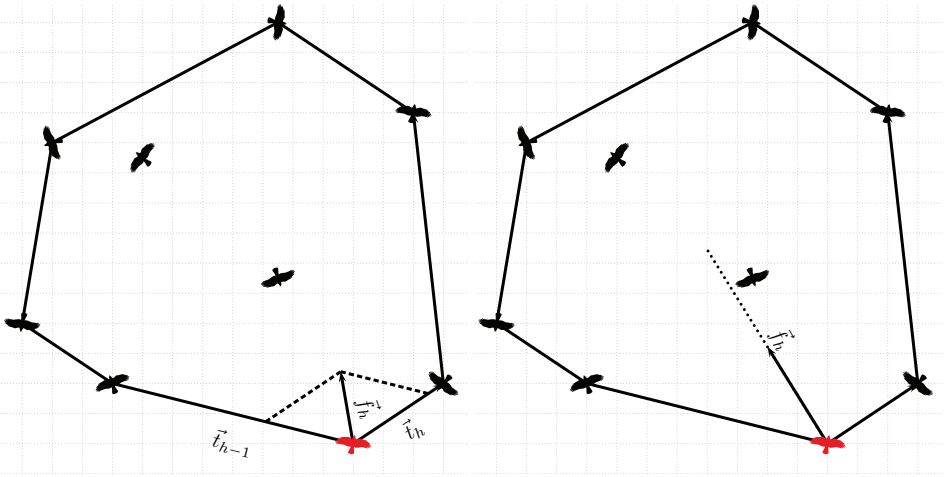

Figure 1.7: *The local curvature (left) and flock mean (right) force recipes visualised. The length of the force vector is not necessarily representative of the actual force as it is implemented.*

Flock Mean

In the flock mean recipe, the boid is forced toward the average position of all boids. It is thus given simply by

$$\mathbf{f}_h = \left(\frac{1}{N}\sum_b \mathbf{r}_b\right) - \mathbf{r}_h \tag{1.25}$$

Far-Neighbour

In the Far-Neighbour force recipe, boids are pointed toward that neighbour on the hull that is furthest away. It attempts to preserve a density, be-

Version of May 31, 2017– Created May 31, 2017 - 17:35

ing at the same time an attractive as well as a repulsive force. It is similar to the Local Curvature recipe, except difference vectors are not normalised prior to use. It is given by:

$$\mathbf{f}_h = 2\frac{\mathbf{t}_{h+1} - \mathbf{t}_h}{|\mathbf{t}_{h+1}| + |\mathbf{t}_h|} \tag{1.26}$$

Near-Neighbour

Where the Far-Neighbour force recipe attempts to preserve the density along the hull by pointing away from the nearest neighbour, the Near-Neighbour recipe does the opposite: it uses the length of the Far-Neighbour recipe, and mirrors it along the direction given by the local curvature force recipe. This way, it is purely an attractive recipe, simulating the wishes of boids to stay close to its closest neighbour on the hull. It is then given by

$$\mathbf{f}_h = \mathcal{M}_{\hat{t}_{h+1},\hat{t}_h}\left[2\frac{\mathbf{t}_{h+1} - \mathbf{t}_h}{|\mathbf{t}_{h+1}| + |\mathbf{t}_h|}\right] \tag{1.27}$$

with $\mathcal{M}_{\hat{v},\hat{w}}[\mathbf{u}]$ a mirroring operator that works by projecting $\mathbf{u}$ on the normal vector

$$\hat{n} = \mathcal{N}[\hat{v} - \hat{w}] \tag{1.28}$$

and on a vector $\hat{n}^\perp$ orthogonal to $\hat{n}$ (chosen such that $\hat{n}^\perp \cdot \mathbf{u} > 0$). Then

$$\mathcal{M}_{\hat{v},\hat{w}}[\mathbf{u}] = \hat{n}(\hat{n} \cdot \mathbf{u}) - \hat{n}^\perp\left(\hat{n}^\perp \cdot \mathbf{u}\right) \tag{1.29}$$

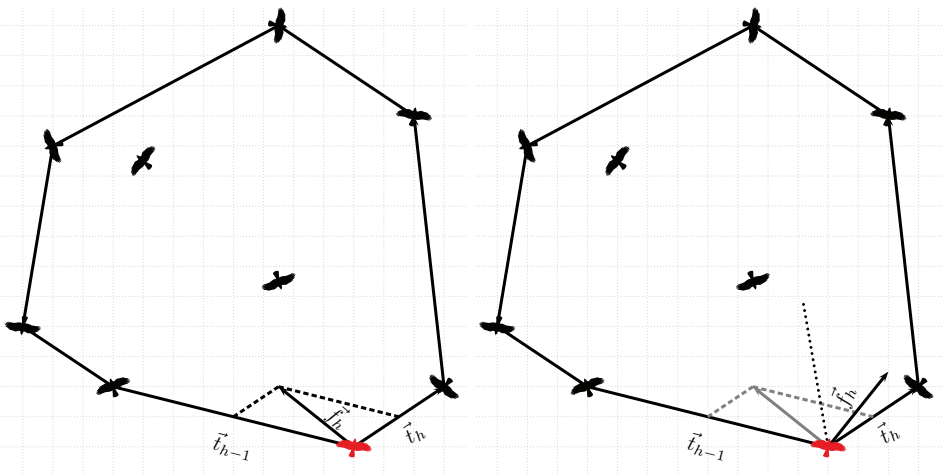

Figure 1.8: *The far-neighbour (left) and near-neighbour force recipes visualised. The length of the force vector is not necessarily representative of the actual force as it is implemented.*

Version of May 31, 2017– Created May 31, 2017 - 17:35

1.4.2 Observables

With the introduction of the convex hull, new possibilities for measurements are also introduced. Aside from measuring the total polarisation $\mathbf{P}_T$ of the flock and its rate of precession κ_T, we can separate these values up into contributions from boids on the hull and boids in the bulk, i.e. those not on the hull. These quantities will be denoted with a subscript H and B respectively and are given by

$$\mathbf{P}_H = \frac{1}{N_H} \sum_h \mathbf{v}_h \tag{1.30}$$

$$\mathbf{P}_B = \frac{N\mathbf{P}_T - N_H\mathbf{P}_H}{N - N_H} \tag{1.31}$$

where N_H is the number of boids on the hull. In principle these polarisations should not differ greatly, as the boids will still be moving in a cooperative fashion, however the force acting on boids on the hull does act as a kind of nontrivial source of noise, even if their contribution is minor: typical simulations of 2000 boids tended to have on the order of 30 to 40 boids on the hull at all times, and so the total polarisation is still affected somewhat. To mitigate this, measurements involving the polarisation or curvature of the flock will be given by those of the bulk unless otherwise noted.
The convex hull itself also introduces the opportunity to perform measurements on its effects: the shape of the hull is usually a good indicator of the shape of the flock as a whole, and the force imparted by the hull affects the positions of boids relative to the bulk. We opted to measure the following properties of boids on the hull, as a function of angular position ϕ (see Fig. 1.9) relative to the centre of the hull, zeroed on the polarisation direction:

- The distance $r_H(\phi)$ of boids to the centre of the hull $\mathbf{r}_{GC}$. This allowed us to construct the shape of the hull, and to compute the length of the perimeter.
- The number of boids $n_H(\phi)$ on the hull. Combined with knowing the shape of the hull, this leads to a local density $\rho_H(\phi)$.
- "Transport" on the hull: if boids stayed on the hull for multiple consecutive timesteps, they made a change $\Delta\phi(\phi)$ in angle relative to the centre of the hull.

All of these measurements were done with histograms of bin size $d\phi = \frac{2\pi}{1000}$.

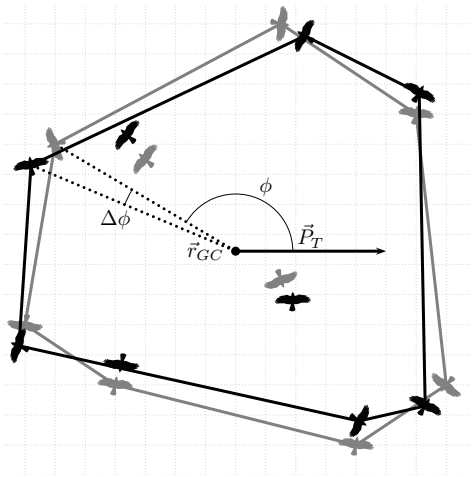

Figure 1.9: *Diagram of how the hull observables' position ϕ is found and how the change in angle was calculated.*

The centre of the hull, however, is typically not best given by the mean geometric mean of all boids or of the boids on the hull, as both are not uniformly spread about the bulk. Instead, we opted to use a measure we will call the Geometric Centre,

$$\mathbf{r}_{GC} = \frac{1}{L_H} \sum_h \left(\mathbf{r}_h + \mathbf{r}_{h+1}\right) \frac{\ell_h}{2} \tag{1.32}$$

where $\ell_h = |\mathbf{r}_h - \mathbf{r}_{h+1}|$ is the distance between consecutive boids on the hull and L_H is the total length of the perimeter of the hull, i.e. $\sum_h \ell_h$.
We measured the surface area of the convex hull by using the "shoe-lace formula:"

$$A = \frac{1}{2} \left| \sum_h \det \begin{pmatrix} x_h & x_{h+1} \\ y_h & y_{h+1} \end{pmatrix} \right| \tag{1.33}$$

Finally, we can reconstruct the forces experienced by Boids on the hull. One way is to calculate the shape of the hull using $r_H(\phi)$ and $n_H(\phi)$, and for each bin, calculate the forces if the neighbouring bins were also populated with a Boid. For a typical hull, this results in a set of force vectors such as in Fig. 1.10.

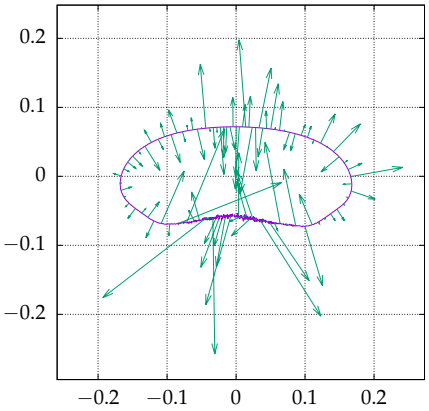

Figure 1.10: *Example of a reconstruction of the forces on the hull, using the local curvature force recipe and purely the shape of the hull.*

Clearly, this method is rather inaccurate and subject to the minute variations in the shape of the reconstructed hull. Furthermore, it distorts the strength of the forces by removing information on the distances between Boids. We can get rid of these errors by instead "placing" the correct number of Boids on the hull with the distribution given by $\rho(\phi)$. This is done by performing an integral $\sigma(\phi', \Phi) = \int_{\phi'+d\phi}^{\Phi} \rho(\phi)\, d\phi$ over the density on the hull, starting at a neighbouring position $\phi' + d\phi$ and ending at the nearest position Φ that gives $\sigma(\phi', \Phi) \geq 1$. We then assume the neighbouring Boid is placed at position Φ, repeat the process on the other side of ϕ' and use those positions to calculate the forces. This gives us the forces found in Fig. 1.11.

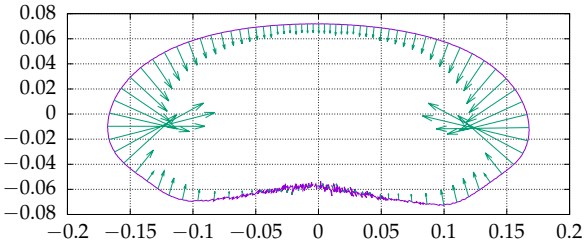

Figure 1.11: *Example of a reconstruction of the forces on the hull, using the local curvature force recipe and taking into the account the density on the hull.*

Version of May 31, 2017– Created May 31, 2017 - 17:35

If we put the flock into a disordered state by raising the noise level beyond a critical value η_C, we can assume Boids to make trajectories that approach a random walk. The equilibrium shape of the convex hull will become circular, and we can make some estimations on the forces experienced by Boids on the hull. From this, we can derive an equation relating the force, noise level and surface area. For this, we need only assume that the shape of the convex hull is a regular polygon with

$$n = \frac{1}{T}\sum_{\phi} n_H(\phi) \tag{1.34}$$

vertices. From this it follows that, in the disordered regime, all force recipes employed in this thesis will point radially inward, and be of equal magnitude at each point on the hull, i.e. $\mathbf{f}_i = -\alpha_F \hat{r}$, with α_F a value dependent on the force recipe employed.
For the local curvature force recipe, we have

$$\mathbf{f}_i = -2\frac{\hat{t}_i - \hat{t}_{i-1}}{|\mathbf{t}_i| + |\mathbf{t}_{i-1}|} \tag{1.35}$$

$$= -2\frac{\left|\hat{t}_i - \hat{t}_{i-1}\right|}{2\left(\frac{2\pi R}{n}\right)}\hat{r} \tag{1.36}$$

Now, as the hull is a regular n-gon, the angle between $\hat{t}_i$ and $\hat{t}_{i-1}$ is

$$\theta = \angle \hat{t}_i \hat{t}_{i-1} = \frac{2\pi}{n} \tag{1.37}$$

From this, we find that

$$\left|\hat{t}_i - \hat{t}_{i-1}\right| = \left|\hat{u} - \mathcal{R}_\theta[\hat{u}]\right| \tag{1.38}$$

with $\mathcal{R}_\theta[\hat{u}]$ a rotation operator. Then

$$\left|\hat{t}_i - \hat{t}_{i-1}\right| = \sqrt{2 - 2\hat{u}\cdot\mathcal{R}_\theta[\hat{u}]} \tag{1.39}$$

$$= \sqrt{2 - 2\cos\theta} \tag{1.40}$$

$$= 2\left|\sin\frac{\theta}{2}\right| \tag{1.41}$$

Plugging in θ, we get

$$\alpha_C = 2\frac{2\left|\sin\frac{\pi}{n}\right|}{2\left(\frac{2\pi R}{n}\right)} \tag{1.42}$$

$$= \frac{\left|\sin\frac{\pi}{n}\right|}{\frac{\pi R}{n}} \tag{1.43}$$

For large n, we can linearise this and get

$$\alpha_C = \frac{1}{R} \tag{1.44}$$

Which is to be expected from a force given by the curvature of the hull.
The Near-Neighbour and Far-Neighbour force recipe calculations are essentially the same, replacing $\left|\hat{t}_i - \hat{t}_{i-1}\right|$ with $|\mathbf{t}_i - \mathbf{t}_{i-1}| = 2\,|\mathbf{t}_i|\left|\sin\frac{\pi}{n}\right|$ and resulting in

$$\alpha_{FN} = \alpha_{NN} = 2\frac{2\left(\frac{2\pi R}{n}\right)\left|\sin\frac{\pi}{n}\right|}{2\left(\frac{2\pi R}{n}\right)} \tag{1.45}$$

$$= 2\left|\sin\frac{\pi}{n}\right| \tag{1.46}$$

$$\approx 2\frac{\pi}{n} \tag{1.47}$$

Finally, the mean position force recipe simply has as magnitude the radius of the hull, i.e. $\alpha_M = R$.
Armed with these expected forces, we can relate the inward force on a boid, $\gamma\,|\mathbf{f}_i|$ to the outward pressure p multiplied by the section of the hull that this boid occupies, $\Delta\ell = \frac{2\pi R}{n}$. This pressure presumably grows as the "temperature" of the flock, or some power of the noise level η. We then have

$$\gamma\,|\mathbf{f}| \sim p\Delta\ell \tag{1.48}$$

$$= \eta^\beta\left(\frac{2\pi R}{n}\right) \tag{1.49}$$

For the local curvature, we then have

$$\frac{\gamma}{R} \sim \eta^\beta\left(\frac{2\pi R}{n}\right) \to n\frac{\gamma}{A} \sim \eta^\beta \tag{1.50}$$

While the Far-Neighbour and Near-Neighbour force recipes would have

$$\gamma\frac{2\pi}{n} \sim \eta^\beta\left(\frac{2\pi R}{n}\right) \to \frac{\gamma^2}{A} \sim \eta^{2\beta} \tag{1.51}$$

and finally the mean position force recipe should follow

$$\gamma R \sim \eta^\beta\left(\frac{2\pi R}{n}\right) \to \gamma n \sim \eta^\beta \tag{1.52}$$

Chapter 2

The simulation

We programmed the simulation using C++ in combination with Qt, a platform-independent interface framework that allows one to easily create an XML-based GUI through drag-and-drop functionality. This enabled us to quickly construct a program that allowed for run-time entry of the system parameters, visualisation of the system, direct plotting of observables and performing a Fast Fourier Transform of these observables where such analysis could prove fruitful.
For further analysis, a history of the observables could be printed to a plaintext data file, while saving checkpoint files containing only the current state allowed us to continue running a particular instance at a later time, or to use a thermalised state with certain parameters as the initial state of another run with similar parameters.
The C++ language, while relatively high-level, is also useful for high-performance computing, which was a requirement to run a large number of instances of the model. In combination with the OpenMP multithreading library, additional speedups could be gained at portions of the code where this was possible, such as interacting boids and updating their positions. Furthermore, the object-oriented nature of the language lends itself to create code that is both compact and efficient.

2.1 The program

To execute the Vicsek model, we needed to turn the rules into a set of programming routines. A large portion of this code is trivially implemented and has a computational complexity of $\mathcal{O}(N)$ to $\mathcal{O}(N \log N)$. Written succintly, the entire program can be written as follows:

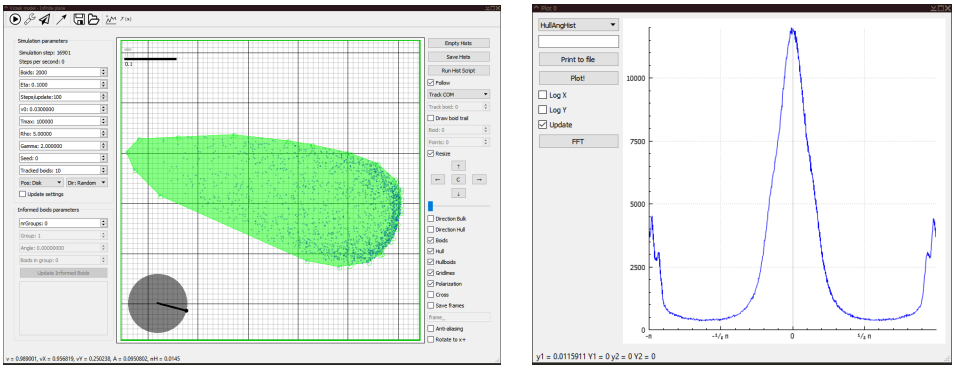

Figure 2.1: **Left**: *A visualisation of the simulation. On the left of the visualisation, model parameters are displayed and can be altered, while on the right there are options for different visual aids such as showing boid directions and histories of positions relative to the center of the hull.* **Right**: *Built-in plot window of time-dependent observables such as the surface area of the convex hull or the curvature, or time-averaged histograms of boids on the hull, such as the change in angle or distance to the geometric center. In this case, a histogram of boids on the hull as function of coordinate relative to the polarisation direction.*

1: Set the initial state
2: Find the Convex Hull
3: Find the polarisations P_T, P_B and P_H
4: **for** T timesteps **do**
5: Interact boids
6: Update boids
7: Find the Convex Hull and update hull histograms
8: Find the new polarisations and curvatures
9: **end for**

We will expound on the portions of the code dealing with interaction, updating of orientation and positon and finding the new convex hull. For the rest of this chapter, boid-specific variables are written, using C++ member variable notation, as "$b.x$", e.g. $\mathbf{r}_b = b.\mathbf{r}$, $\mathbf{v}_b = b.\mathbf{v}$, etc.

2.1.1 Interaction algorithms

The Interaction algorithm, which entails checking pairs of boids (b, b') for their distance $r_{b,b'} = |\mathbf{r}_{b,b'}| = |b.\mathbf{r} - b'.\mathbf{r}|$, can be implemented in multiple ways and will offer the most gains in terms of speed when programmed

optimally, as the remainder of the code has a complexity of $\mathcal{O}(N \log N)$ at the worst (caused by the algorithm that finds the convex hull). We will explain all three of the algorithms used in this section.

Brute-force algorithm

The brute-force algorithm is an easily implemented way of running the Vicsek model, whereby each individual boid b checks the distance $r_{b,b'}$ between every boid b' (including itself). If $r_{b,b'}(t) \leq \ell_0$, the boids "interact", i.e. boid b adds the velocity vector $b'.\hat{v}(t)$ of b' to a temporary vector $b.\mathbf{sumV}$ and increments its variable $b.numNeighbours$ by one. In pseudocode, this algorithm can be written in the following way:

```
1: for Each boid b do
2:     for Each boid b' do
3:         if |r_bb'| ≤ ℓ_0 then
4:             Add b'.v to b.sumV
5:             Increment b.numNeighbours by 1
6:         end if
7:     end for
8: end for
```

While the original paper by Vicsek et al. states that the angle θ is averaged to find the new direction, this method removes the need for computationally costly operations to find the angle from Cartesian coordinates and properly averaging this to find the new direction: one need now only normalise $\mathbf{sumV}$ when all boids have been considered, add noise and the new direction is found.
Whatever the exact way of finding the new direction may be, this algorithm has a complexity of $\mathcal{O}(N^2)$. If, rather than allowing each boid b to consider every boid b', b were to consider only boids b' that themselves have not yet looked for neighbours, the runtime could be halved by adding $b.\mathbf{v}(t)$ to $b'.\mathbf{sumV}$ and $b'.\mathbf{v}(t)$ to $b.\mathbf{sumV}$ at the same time. Nevertheless, this algorithm would still be of complexity $\mathcal{O}(N^2)$, which makes running large systems or probing a large portion of the parameter space in reasonable time intractable. Luckily, there is another way, which produces the exact same results without sacrificing precision.

Box algorithm

Like in many simulations where the interaction range varies with a distance metric, we can implement a better way to handle our model. In $N-body$ simulations where the interaction falls off smoothly, this can be accomplished by approximations such as the Barnes-Hut tree, which partitions the system into cells with a center of mass given by the particles inside it. For particles whose distance from this center of mass is larger than a certain threshold, the contributions of individual particles in the cell can be replaced by a single term, resulting in an algorithm of $\mathcal{O}(N \log N)$ complexity. Implementing this algorithm is quite involved, however, and in the case of the Vicsek model, unnecessary. As the interaction immediately falls away when two boids are further removed than ℓ_0, we can instead subdivide the system into boxes of size ℓ_0^2. This way, each boid need only consider those boids that are in the same box, and those boids that are in boxes neighbouring its own box. Under ideal circumstances, this also results in $\mathcal{O}(N \log N)$ performance. In pseudocode, this algorithm is given by

```
1:  for Each box B do
2:    for Each boid b do
3:      for Each boid b′ ∈ B do
4:        if |r_bb′| ≤ ℓ_0 then
5:          Add velocity b′.v to b.sumV
6:          Increment b.numNeighbours by 1
7:          Add velocity b.v to b′.sumV
8:          Increment b′.numNeighbours by 1
9:        end if
10:     end for
11:   end for
12:   for each of 2^d specific neighbouring boxes B′ do
13:     for Each boid b ∈ B do
14:       for Each boid b′ ∈ B′ do
15:         if |r_bb′| ≤ ℓ_0 then
16:           Add velocity b′.v to b.sumV
17:           Increment b.numNeighbours by 1
18:           Add velocity b.v to b′.sumV
19:           Increment b′.numNeighbours by 1
20:         end if
21:       end for
22:     end for
23:   end for
```

24: **end for**
25: [Update locations]
26: **for** Each boid b **do**
27: Add reference to b to box $B_{b.\mathbf{r}_x, b.\mathbf{r}_y}$
28: **end for**

where the sum over neighbouring boxes is such that each pair of boxes is only considered once, much like in the Ising model one can choose to sum only over half the neighbours and still obtain each term: see Fig 2.2.

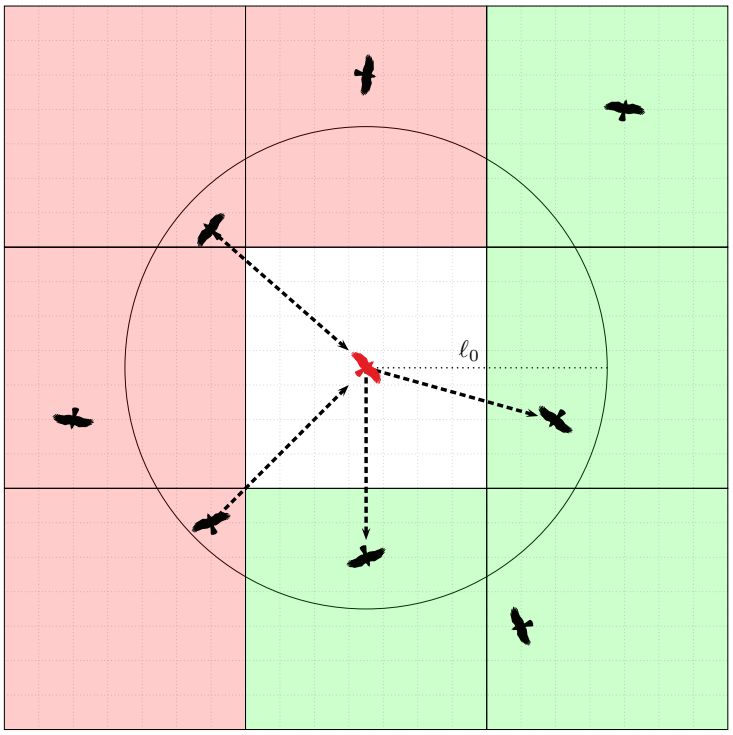

Figure 2.2: *The box interaction algorithm visualised. Boids in the center box itself compare distances with boids in boxes coloured green, while boids in boxes coloured red compare distances with boids in the center box.*

An additional ring of empty boxes is placed around the system to avoid addressing invalid memory while looping over neighbouring boxes. We ran the model on both algorithms with full noise to study the time required per step and found performance as expected. This can be seen in Fig 2.3.

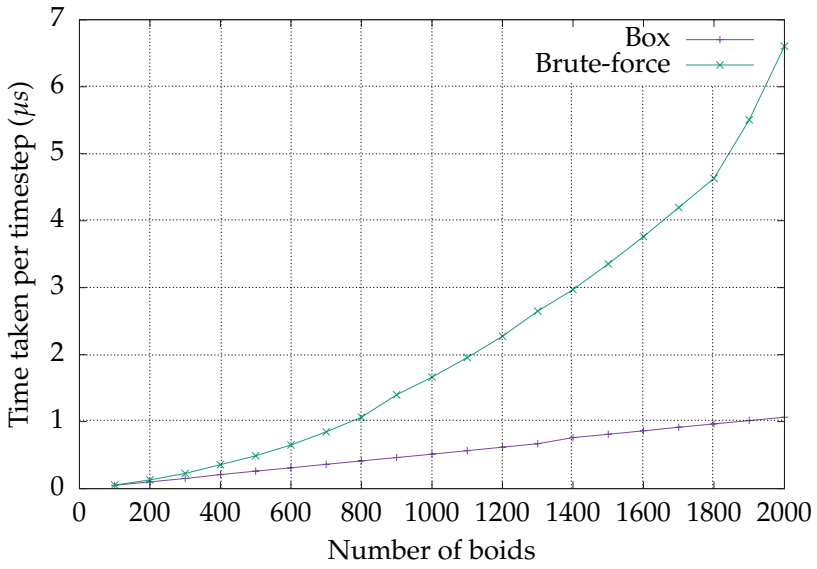

Figure 2.3: *Time required to compute a timestep with both algorithms for various numbers of boids*

While possibly a vastly superior algorithm compared to the Brute-force implementation, there are two caveats:

- For extremely sparse systems, the algorithm will waste time running over empty boxes, again increasing the amount of time required to complete a single timestep.
- For extremely dense systems, the algorithm reduces to $\mathcal{O}\left(N^2\right)$ performance, if a large fraction of the boids is concentrated within an area of size $\sim \ell_0^2$.

As our system has a convex hull forcing boids to coalesce, the first situation is not an issue and can only happen during thermalisation with a very low initial density. The second situation, on the other hand, occurs in most positions of the parameter space: only in the case of a disordered system does the majority of boids not coalesce in a small region. For a typical equilibrium state in the ordered regime, we found that the surface area of the convex hull was on the order of ℓ_0^2, if not smaller.

Full Interaction Algorithm

There is a trick, however, that allows us to vastly speed up computation in some of these high-density cases: for a low enough level of noise, the

largest separation between boids is actually smaller than ℓ_0, meaning all boids have the same average direction after the interactions have taken place. This means we can simply replace the entire algorithm of interaction by using the polarisation vector from the previous timestep, resulting in an algorithm of complexity $\mathcal{O}(N)$:

---

for Each boid b **do**
  Set $b.\mathbf{sumV}$ to $N \cdot \mathbf{P}_T(t-1)$
  Set $b.numNeighbours$ to N
end for

2.1.2 Updating positions

After all boids have interacted, updating the positions consists almost entirely of adding a form of noise to the boid's local average direction and applying the force if the boid is on the hull. For the box algorithm, some additional operations are required to keep the dimensions of the array of boxes correct. Updating the positions of boids is inherently an operation of linear complexity, and can at most be improved upon by multithreading the operations.

---

for Each boid b **do**
  if Using "Scalar noise" **then**
    Compute new direction $\theta_b = \arctan 2\left(b.\mathbf{sumV}_y, b.\mathbf{sumV}_x\right)$
    Add error term $\eta\xi_b$ to θ_b
    Set $b.\mathbf{v}$ to normal vector $\hat{n}(\theta_b) = \begin{pmatrix} \cos\theta_b \\ \sin\theta_b \end{pmatrix}$
  else
    Add error vector $\eta \cdot b.numNeighbours \cdot \hat{n}(\xi_b)$ to $b.\mathbf{sumV}$
    Normalise $b.\mathbf{sumV}$
    Set $b.\mathbf{v}$ to $b.\mathbf{sumV} + \gamma \cdot b.\mathbf{f}$
    Normalise $b.\mathbf{v}$
  end if
  Add $v_0 \cdot b.\mathbf{v}$ to $b.\mathbf{r}$
  if $b.\mathbf{r}_x < x_{min}$ **then**
    Set x_{min} to $\lfloor b.\mathbf{r}_x \rfloor$
  else if $b.\mathbf{r}_x > x_{max}$ **then**
    Set x_{max} to $\lceil b.\mathbf{r}_x \rceil$
  end if

18: **if** $b.\mathbf{r}_y < y_{min}$ **then**
19: Set y_{min} to $\lfloor b.\mathbf{r}_y \rfloor$
20: **else if** $b.\mathbf{r}_y > y_{max}$ **then**
21: Set y_{max} to $\lceil b.\mathbf{r}_y \rceil$
22: **end if**
23: Set b.**sumV** to zero vector
24: Set b.**force** to zero vector
25: Set $b.numNeighbours$ to 0
26: **end for**
27: Create new system of $x_{max} - x_{min} + 2$ by $y_{max} - y_{min} + 2$ boxes

2.1.3 Finding the new convex hull

Finally, the updated system requires the convex hull to be calculated again, which is done using Andrew's Monotone Chain Algorithm[18], of complexity $\mathcal{O}(N \log N)$. After constructing the hull, forces can be calculated, as well as the different polarisation vectors and the curvature. Additionally, by looping only over boids on the hull, information on the shape of and transport on the hull can be gained.

1: Sort *boids* lexicographically
2: **for** Each boid b, increasing in lexicographical order **do**
3: **while** $|H| \geq 2$ **&&** $\angle H_{|H|}.\mathbf{r}\ H_{|H|-1}.\mathbf{r}\ b.\mathbf{r}$ is not counter-clockwise **do**
4: Remove $H_{|H|}$ from H
5: **end while**
6: Append b to H
7: **end for**
8: **for** Each boid b, decreasing in lexicographical order **do**
9: **while** $|H| \geq 2$ **&&** $\angle H_{|H|}.\mathbf{r}\ H_{|H|-1}.\mathbf{r}\ b.\mathbf{r}$ is not counter-clockwise **do**
10: Remove $H_{|H|}$ from H
11: **end while**
12: Append b to H
13: **end for**
14: **for** Each boid $b \in H$ **do**
15: Calculate b.**f**
16: Calculate the angle θ_b that b makes relative to $\mathbf{r}_{GC}$ w.r.t. θ_{P_T}
17: Update histograms in the bin containing θ_b
18: **end for**
19: Remove last entry in H

Version of May 31, 2017– Created May 31, 2017 - 17:35

Now, as said, this algorithm of complexity $\mathcal{O}(N \log N)$, which is due to the sorting of boids by x-position (and by y-position if two boids have the same x-position). The standard $C++$ implementation sorting algorithm is guaranteed to have $N \log N$ performance, and so we can expect this to be the case for the entire algorithm, as all other operations happen in linear time.

Chapter 3

Results

In this chapter, we present the results of our simulations. These results are divided chiefly into the force recipe employed. Within those sections, we further divide up the results into those gained from states wherein the polarisation of the bulk approached unity, i.e. the system was moving collectively, and those disordered states wherein the polarisation vanishes. This disorder was induced purely by raising the noise level η beyond the critical value of $\eta_C \approx 0.66$, removing the possibility for local order, rather than by putting the value of γ on a suitably low value to allow the convex hull to balloon to arbitrary size. We will first present the order parameter P_B as function of noise level for various force constants to compare against the results of the model with periodic boundary conditions.
After this, results on the convex hull, such as its shape and size, local density and transport will be presented. Finally we present the effects of noise on the direction of the flock.
Each section concludes with the results of the disordered regime, showing the dependence of the surface area A on the two control parameters η and γ. After this, a short conclusion on the force recipe is given.
In the Far-Neighbour recipe, we present additional results pertaining to a novel behaviour found exclusively using that mechanism: the properties of the rotational state.
Dimensions are scaled to interaction radii ℓ_0, e.g. speeds are in ℓ_0 per timestep, lengths in ℓ_0 and area in ℓ_0^2. Unless otherwise noted, the number of boids in the simulation N was set to 2000, the initial number density ρ to $5.0\ell_0^{-2}$, the speed of the boids $v_0 = 0.03\ell_0$ per timestep and the boids were distributed uniformly on a disk with radius $R = \sqrt{\frac{N}{\pi\rho}}\ell_0$, with uniformly random initial directions.

Version of May 31, 2017– Created May 31, 2017 - 17:35

Simulations were run by either (i) setting the parameters, allowing it to thermalise for $2 \cdot 10^5$ timesteps, clearing all data and running it again for 10^5 timesteps or (ii) loading a state with similar parameters, allowing it to thermalise for 10^5 timesteps, clearing all data and running it again for 10^5 timesteps.

3.1 Local Curvature

3.1.1 Ordered regime

Using the local curvature as a means of keeping the flock intact, we found that noise levels below $\eta = 0.3$ caused the majority of the flock to converge to a very small point, forming a circular front, but keeping 2 boids trailing ever further behind, as shown in Fig. 3.1. This happens quickly after the flock reaches full polarisation, while the shape of the flock is not yet equilibriated: boids on the rear segment of the hull are pushed inward, sharpening the shape of the rear.
As fewer and fewer boids form the convex hull on this segment, those boids remaining will experience their force pulling them to the sides, rather than to the centre of the hull. Ultimately, two boids, very closely together and essentially mirrorring their directions along the polarisation, will permanently be slightly deflected, causing them to move slower relative to the boids in front of them. This effect does not diminish, as the width of the front cluster of boids reaches a finite value by means of the transverse spread induced by the noise.
Conversely, at the front of the flock, those boids forming the hull will also feel a slight lateral force, allowing the bulk of the boids to catch up. They will then lag behind slightly as well, moving along the hull to the back of this cluster, until being pushed off the hull and moving forward unencumbered, repeating the cycle.
As a result of this effect, measurements on the shape of the convex hull were not representative of the behaviour of the bulk of the flock, and the box algorithm was reduced to running in $\mathcal{O}\left(N^2\right)$ speed. Because of this, we focussed only on combinations of parameters with $\eta = 0.3$ and higher, as this allowed the boids to stay together.

Version of May 31, 2017– Created May 31, 2017 - 17:35

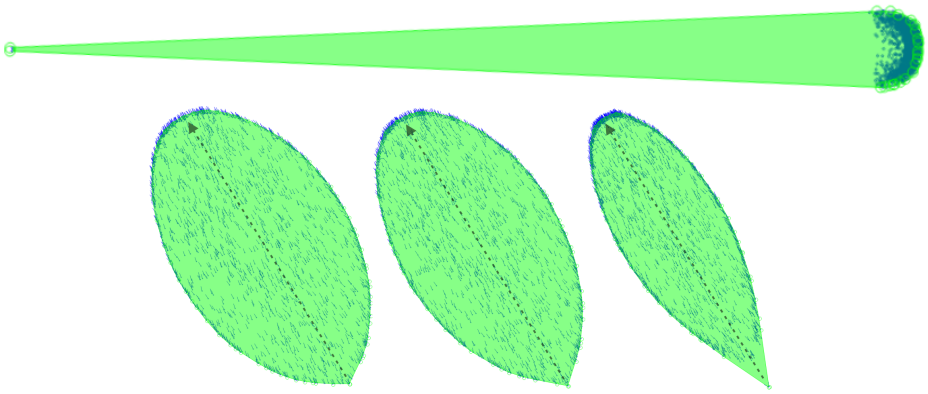

Figure 3.1: *The local curvature force recipe's effect on the shape of the convex hull.* ***Top****: the flock becomes mostly concentrated at the front of the hull, with the exception of two boids at the back trailing behind. The distance between these two boids and the bulk of the flock increases permanently, as the width of the flock reaches a finite value, which in turn is given by the transverse spread in position as a result of the noise.* ***Bottom****: The steps during which this occurs: as the width of the flock decreases, the number of boids at the back of the flock that are on the convex hull decreases. These boids are then allowed to assume the direction of polarisation. At some point, two boids will form a spike, as the force gives them a slight transverse direction. This causes them to permanently lag behind the bulk. The dashed line with the arrow is a guide for the eye to show the symmetry axis, and the polarisation.*

Turning our attention to the noise levels that kept the convex hull in a representative state, we first plot the polarisation as function of noise level, for various force constants in Fig. 3.2.

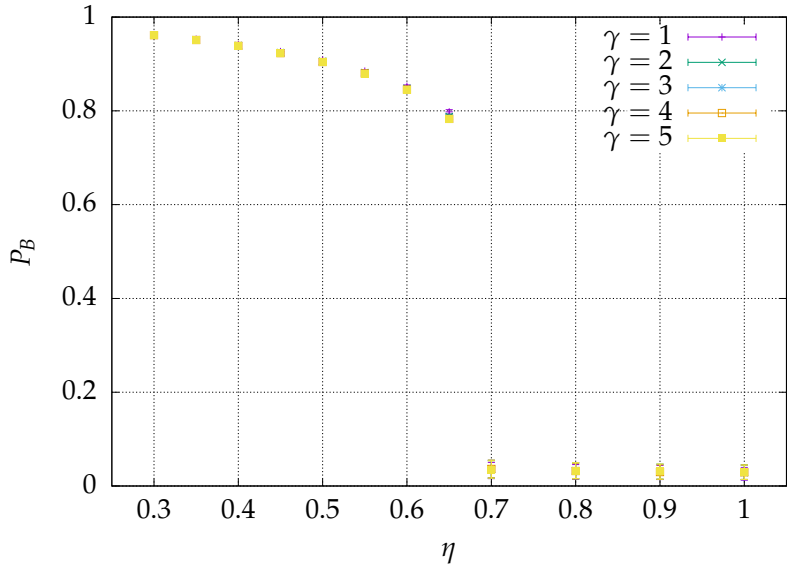

Figure 3.2: *Order parameter P_B as function of noise level η, for various force constants γ, using the local curvature force recipe.*

As can be seen, the polarisation is very weakly dependent on the force constant, but the overall behaviour is not different from that found in the original Vicsek model employing vectorial noise: a sharp transition occurs around $\eta_C \approx 0.66$, between an ordered state and a disordered state.
Next, we present the shape of the convex hull as it was during simulations for various combinations of force constants and noise levels. In Fig. 3.3, we show the shape of the hull, colour-coded to the density of boids. In this force recipe, the front (i.e. the side that points toward the direction of motion) is placed at the top.

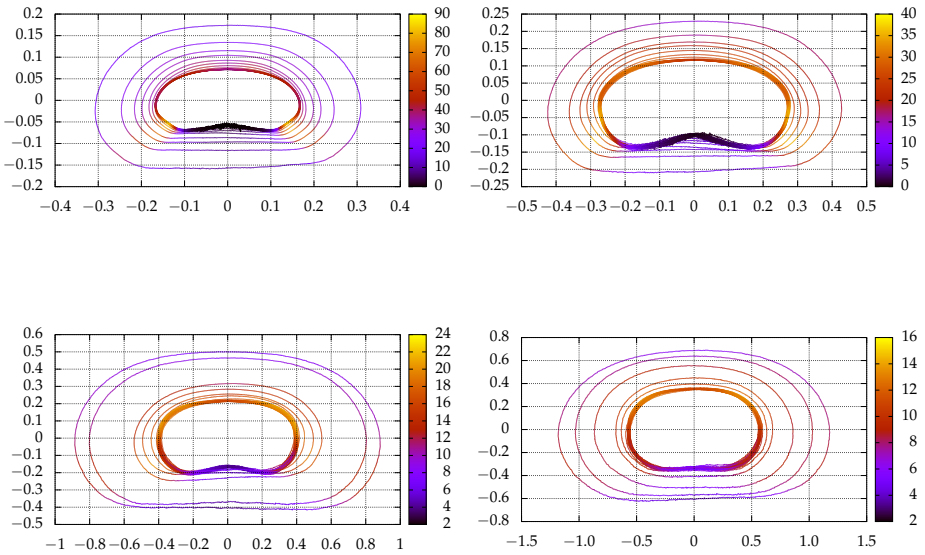

Figure 3.3: *Shape of the convex hull, colour-coded to Boid density $\rho(\phi)$, for varying noise levels, with the polarisation pointing up. Each figure contains plots for multiple force constants, starting at various values γ_{min} and ending at $\gamma = 10$, where the higher force constants settled to a smaller hull.* ***Top left****: $\eta = 0.3$, $\gamma_{min} = 0.0625$,* ***top right****: $\eta = 0.4$, $\gamma_{min} = 0.125$,* ***bottom left****: $\eta = 0.5$, $\gamma_{min} = 0.225$,* ***bottom right****: $\eta = 0.6$, $\gamma_{min} = 0.45$*

In Fig. 3.4, we plot the shape of the hull again, with colours now indicating the transport of boids along the hull, to the back. In this force recipe, we use the absolute value of $\Delta\phi\,(\phi)$, to negate the sign difference between both sides of the polarisation direction. Furthermore, we plot force vectors on the smallest and largest convex hulls, based on the found densities on the hull.

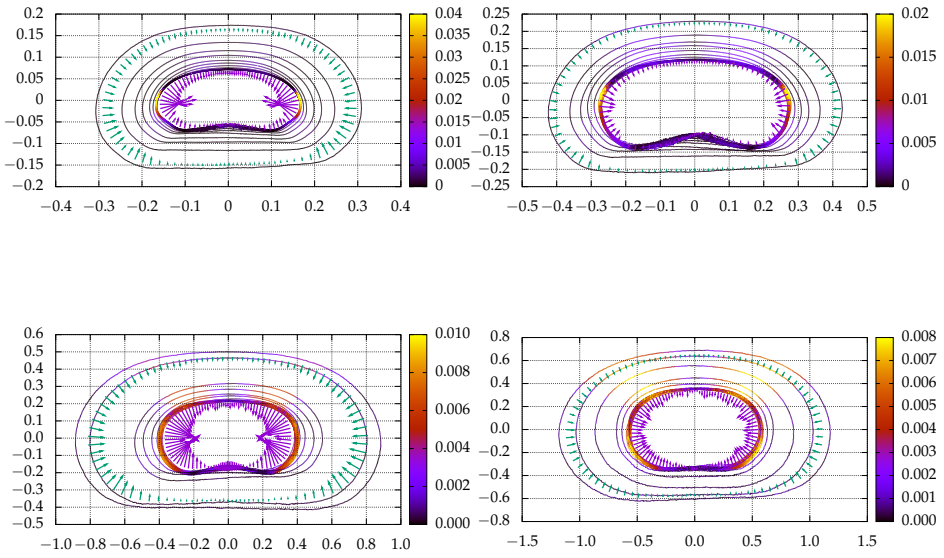

Figure 3.4: *Shape of the convex hull, colour-coded to Boid transport* $v_{Hull}(\phi) = \left|\overline{\Delta\theta}(\phi)\right| \bar{r}(\phi)$. *We also plot the force vectors for 2 hulls, normalised to only represent relative strength as it relates to the local curvature. The layout is the same as in Fig. 3.3*

The first thing we must explain is the overal shape of the hull. In any strongly polarised state of the Vicsek model, the noise added to a Boid's new direction affects mainly the component transverse to the polarisation direction, and so slightly reduces the group velocity parallel to the polarisation. Thus, we can expect the flock to move somewhat slower than the absolute Boid velocity, and to find a larger spread in positions of Boids transverse to the direction of motion. The reduced flock speed also gives way to the possibility for Boids at the back to move toward the front, if their movement is roughly parallel to the direction of motion in multiple consecutive timesteps. The convex hulls found in the local curvature force recipe reflect this, as they are larger in the transverse direction, and tracking single Boids as they moved through the flock revealed some noisy circulatory effects, allowing Boids to visit all positions in the hull if given enough time.
We can see that the density at the back of the hull is lowest. This is due to the fact that (i) Boids at the back of the hull experience a force roughly toward the direction of motion, and so are unable to linger for an extended amount of time, and (ii) Boids that are moving opposite to the direction of motion for a single timestep are usually entirely swayed to move forward

the next timestep, before ever reaching the back. In the lower noise levels, there is also an apparent concave section at the back of the flock for high force constants. This is not actually the shape of the convex hull at any point during the simulation, rather it is a result in the variability of the direction of the polarisation distorting the angle ϕ that the boids on the hull make. As can be seen in the variable distance to the centre of the convex hull, these sections of the hull were sparsely populated relative to the front and sides of the hull, and so the distortion is more prominent here compared to the front and sides.

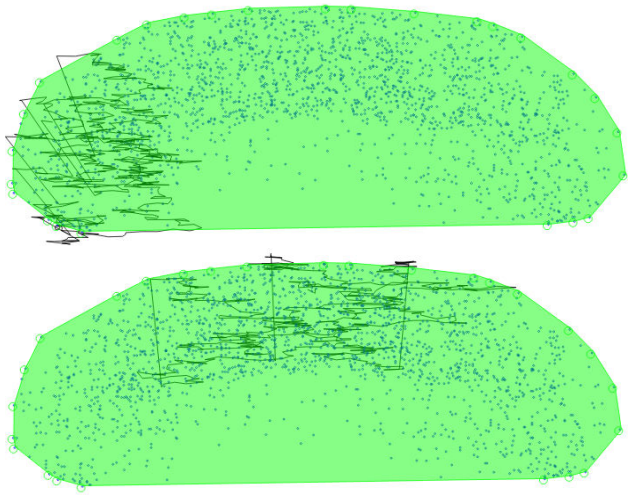

Figure 3.5: *Snapshots of the convex hull (polarisation pointing up) with $\gamma = 10$ and $\eta = 0.30$, with a time trace of 500 relative positions of two separate boids showing the possibility for boids to become trapped at the sides. The points outside the convex hull are not indicative of a boid being outside the hull. Rather, it shows the variable natures of the shape of the convex hull and the direction of motion.*

For $\eta = 0.30$, we find that the front, though visited much more often than the back, is still relatively sparse compared to the rear sides of the hull. This is a result from the reduced freedom of motion a Boid experiences while moving in the side of the bulk, as its transverse movement through the bulk to the front is constrained to mostly moving to the centre. If a Boid does happen to move further toward the side, it is quickly deflected toward the rear side of the hull, while the bulk moves further with enough distance for this single deflection to result in a place on the rear side of the hull. Being released from the hull again, the Boid again finds its movement constrained, and so it becomes trapped at the sides for multiple timesteps, often visiting the hull at this region and thus increasing its density. Conversely, the centre of the hull is somewhat longer

in the direction of motion, and so the deflection at the front generally results in an unencumbered diffusion to the front, which happens on a larger timescale. Both these circulatory phenomena are shown in Fig 3.5.
As the noise level is increased, the size of the hull is increased transversely purely by an increasing transverse spread. The lateral movement is more strongly affected because of this, which diminishes the effectiveness of forward circulation once a boid has been deflected to the back. The density on the hull lowers because of this increase in size, and the length of the hull in the direction of motion increases, giving rise to more paths leading from the side to the front.
In Fig. 3.6, we plot the surface area of the convex hull as function of force constant and as function of noise level. As a function of γ, this saturates at a certain value, given by the noise level. The dependence of this saturation level is plotted as well, where, at least in the lower noise regime, there appears to be a power law with exponent 3.5.

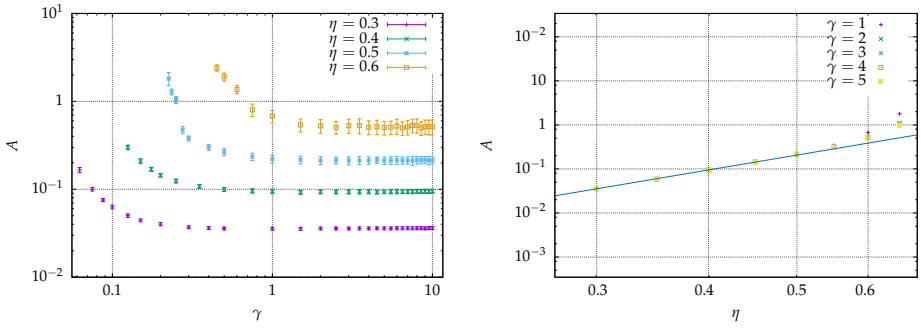

Figure 3.6: Left: *Surface area A as function of force constant γ for various noise levels.* ***Right:*** *Surface area A as function of noise level η for various force constants. The power law drawn corresponds to an exponent of 3.5*

While the mean of the curvature itself vanishes for all instances (i.e. no consistent precession occurs), higher levels of noise ($\eta = 0.4$ and up) cause the flock to drastically readjust its direction of motion in some $\sim$1000 timesteps, a feature inherent to the Vicsek model. In Fig. 3.7, we present some snapshots of the flock as this occurs. Initially, the distribution of boids in the bulk becomes asymmetrical along the direction of polarisation. In turn, the density of Boids on the hull reflects this, and the curvatures at the sides start to differ strongly, triggering a turn toward the side with highest curvature. This rapid change in direction at the hull occurs on a comparable timescale to the bulk's ability to diffuse into a symmetric shape and uniform direction, and so the flock is often subjected to these phenomena, resulting in an often changing direction of motion.

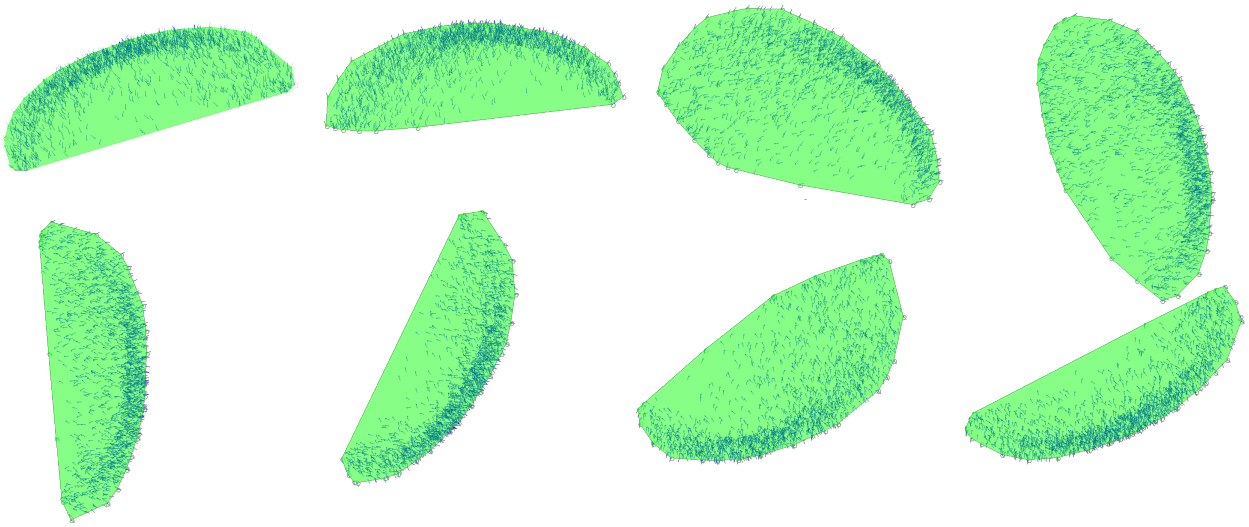

Figure 3.7: *Snapshots of the convex hull with $\gamma = 10$ and $\eta = 0.50$, taken every 400 timesteps during a change in direction, starting at the top left and going right each row.*

In Fig. 3.8, we plot the mean squared value of the bulk's curvature, $\langle \kappa_B^2 \rangle$. This value increases as the noise level grows, reflecting the increasing variability in direction that the flock takes. For the most part, this behaviour is unaffected by the force constant, though values start diverging as the noise is driven up.

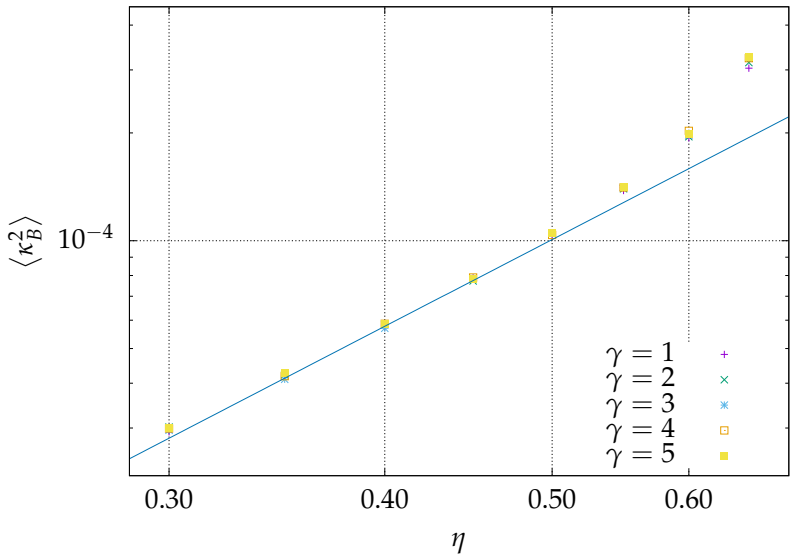

Figure 3.8: *Average squared bulk curvature $\langle \kappa_B^2 \rangle$ as function of noise level for multiple force constants. The power law corresponds to an exponent of 2.5.*

Combining the dependence of A and $\langle \kappa_B^2 \rangle$ on η, we plot in Fig. 3.9 the surface area as function of squared curvature. Curiously, the exponent in this power law is not the difference between the exponents of $A\,(\eta)$ and $\langle \kappa_B^2 \rangle\,(\eta)$, indicating some hidden behaviour that cannot be attributed to the noise level alone.

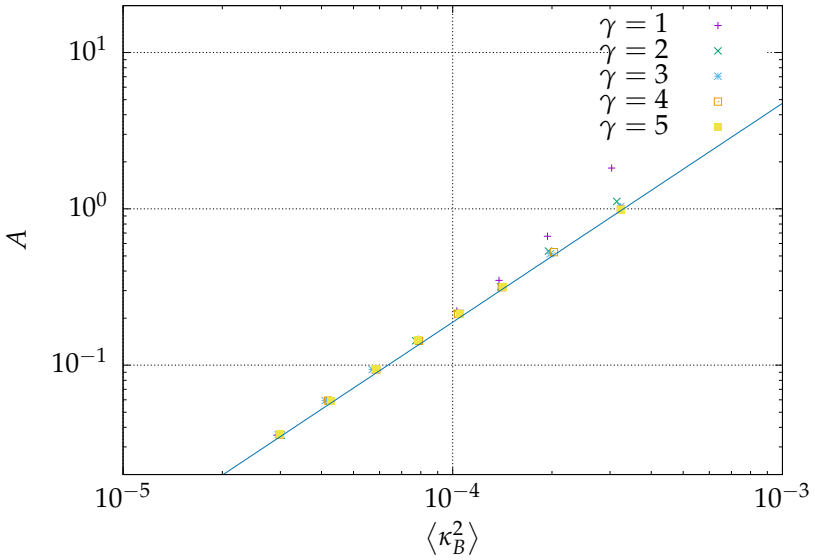

Figure 3.9: *Surface area A as function of average squared bulk curvature $\langle \kappa_B^2 \rangle$. The power law corresponds to an exponent of 1.4.*

3.1.2 Disordered regime

Finally, we present the results of the behaviour of the local curvature recipe when the system is in a disordered state. We induced this disorder purely by raising the noise level above the critical value of $\eta_C \approx 0.66$, rather than lowering the force constant such that the density of the system becomes suitably low for global disorder while allowing local order. In this regime, the convex hull becomes roughly circular (as seen in Fig. 3.10) in shape, and no net motion occurs, up to some random walk behaviour.

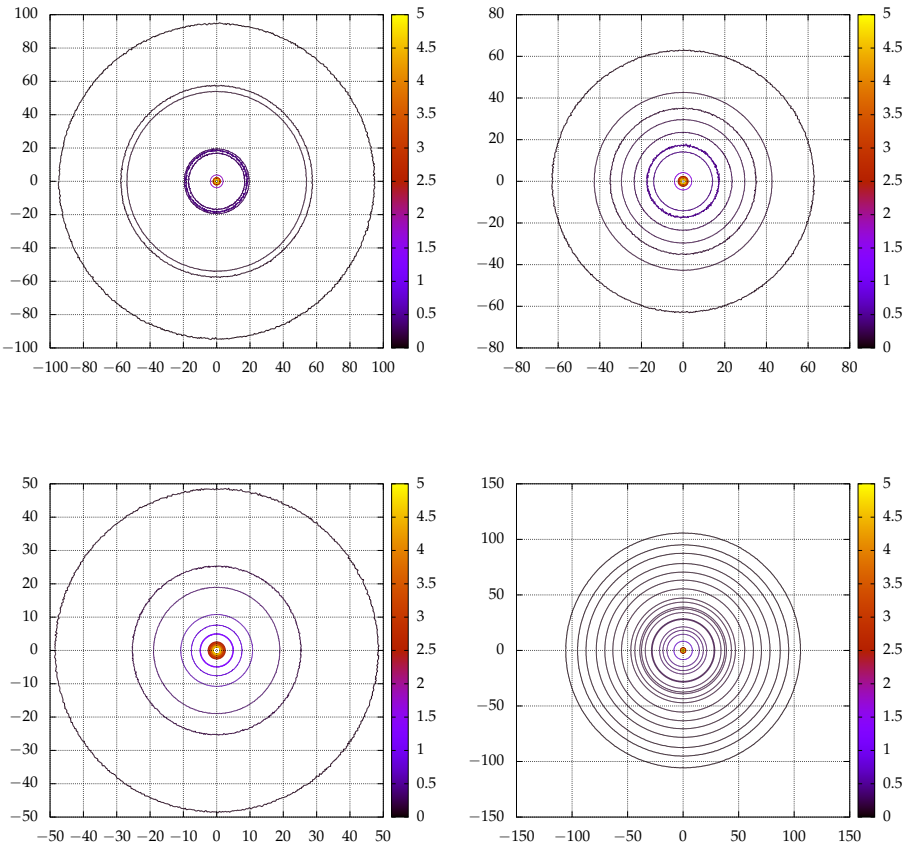

Figure 3.10: *Shape of the convex hull, colour-coded to Boid density $\rho(\phi)$ for varying noise levels above the critical value. Each figure contains plots for multiple force constants, starting at values $\gamma = 0.5$ and ending at $\gamma = 1000$, where the higher force constants settled to a smaller convex hull.* ***Top left:*** *$\eta = 0.7$,* ***top right:*** *$\eta = 0.8$,* ***bottom left:*** *$\eta = 0.9$,* ***bottom right:*** *$\eta = 1.0$.*

In Fig. 3.11, we plot the surface area of the convex hull as function of force constant, for various noise levels.

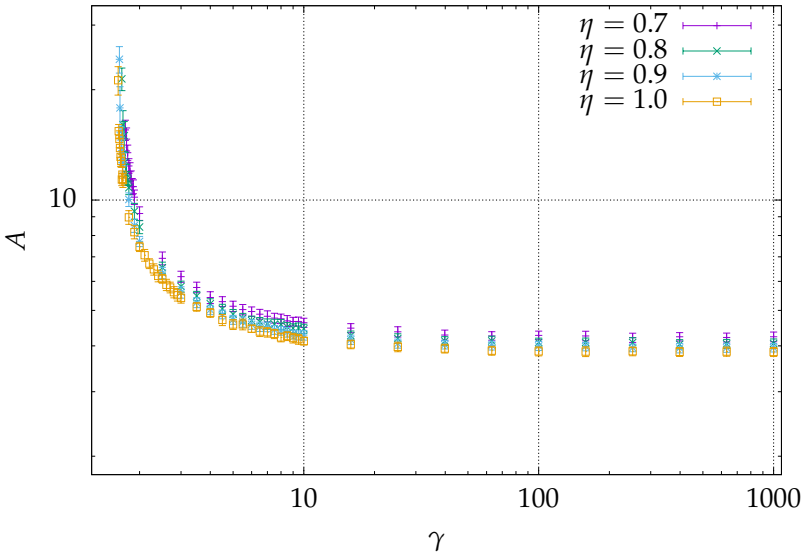

Figure 3.11: *Surface area as function of force constant for various noise levels in the disordered regime, using the local curvature force recipe.*

As γ is increased, the surface area of the flock becomes of order ℓ_0^2 and the giant density fluctuations die out. Though Boids do not have an excluded volume in this model, the result is that the flock becomes "incompressible" and the convex hull settles to a minimum value, dependent on the noise level.
Strangely, we see that the surface area is greatest when the noise level is lowest, which may seem contradictory if we view the noise as analogue to the temperature of the system. The cause of this lies in the fact that raising the noise level in the disordered regime amounts to lowering the persistence length ℓ_p of Boids' trajectories as $\ell_p \sim \eta^{-2}$[19]. As a result, their ability to "push out" against the convex hull in consecutive timesteps is reduced, and the surface area is lowered at the same force constant.
In Fig. 3.12, we plot the surface area of the convex hull as function of noise level for various force constants.

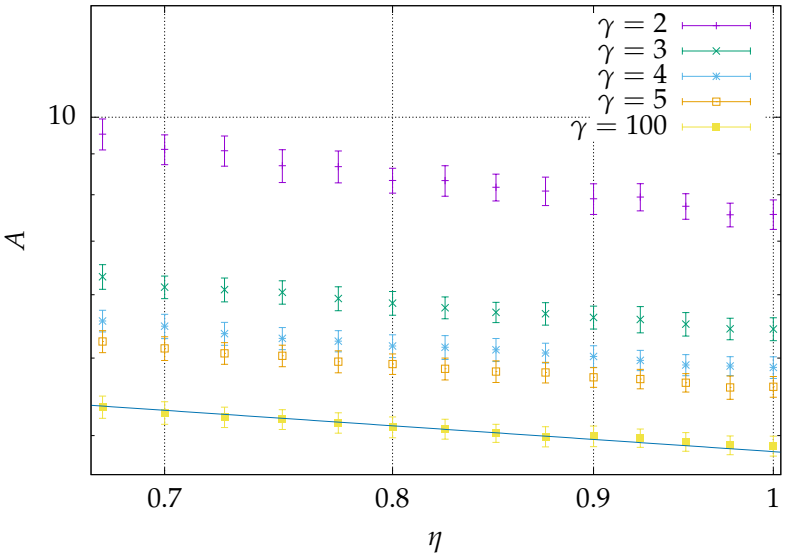

Figure 3.12: *Surface area as function of noise level above η_C for various force constants, using the local curvature force recipe. The power law has exponent $-\frac{1}{3}$.*

We find a relation $A \sim \eta^{-\frac{1}{3}}$. This is surprising: one usually associates a relationship of $p \sim T \sim \text{var}\eta$, or $A \sim \eta^{-2}$. One explanation could be the fact that our assumption that n stays constant is incorrect: in fact, n does scale with A, as can be seen in Fig. 3.13

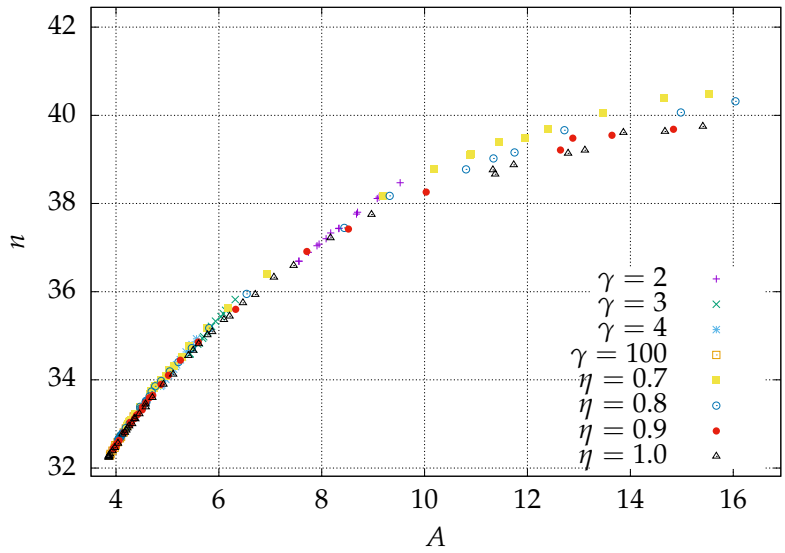

Figure 3.13: *Number of Boids n on the hull as function of surface area A for several instances in the disordered regime using the local curvature force recipe.*

This should not be surprising: as the surface area increases, so too must the convex hull's perimeter, and in turn, so must the number of Boids on the hull, lest the flock's distribution of Boids change. In the end, we cannot properly explain why the surface area scales with η in the way that it does. In order for the relationship $\frac{\gamma n}{A} \sim \eta^2$ to hold for $A \sim \eta^{-\frac{1}{3}}$, n must scale as A^{-5}, which it decidedly does not.
Another possibility is that the pressure of the flock is not given by a power law in η, which would be equally surprising. To compare, we plot in Fig. 3.14 the fit of a linear function and find a coefficient of -1.35.

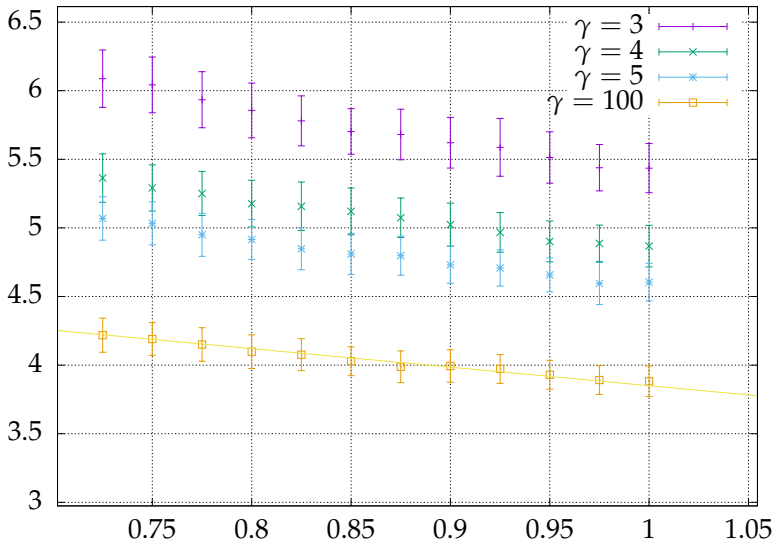

Figure 3.14: *Surface area as function of noise level above η_C for various force constants, using the local curvature force recipe. The coefficient for the fit is -1.35.*

This too, appears to reproduce the behaviour of the flock, at least in this regime of η, and therein lies the problem: in order to show the existence of a scaling law, multiple orders of magnitude in area need to be probed to properly see the relation. Perhaps with careful fine-tuning of the value of γ, or an increase in the number of Boids, this can be realised.

3.1.3 Conclusion

The local curvature recipe presents a mechanism to simulate the flocking behaviour of the Vicsek model in the infinite plane based on the minimisation of local curvature, much like the surface tension of a liquid droplet

is minimised when it assumes its optimal shape. We have shown the dependence of this shape on the force constant γ and the noise level η, and presented some qualitative findings on the motility of Boids in the bulk. While the observables we used were able to capture this, there are phenomena that are better examined by introducing more measurements on the behaviour of the bulk: both the distribution of density and velocity of Boids in the bulk are not properly reflected by those on the hull, as the snapshots in Fig. 3.5 display a definite arc of high density. One shortfall of this force recipe is its inability to coalesce the flock at low noise levels, precluding probes into the behaviour below $\eta = 0.3$. Furthermore, the reaction of the convex hull to changes in direction actually amplify this behaviour. In order to properly capture the relationship between noise level and surface area, far greater system sizes must be simulated.

3.2 Flock Mean

The Flock Mean force recipe grants Boids an ability that is usually not given: the means to detect a global quantity of the flock. In this way, it stands out, compared to the other force recipes. Superficially, however, it behaves similarly to the previous force recipe, in that Boids are kept together in a flock that is spread out more in the transverse direction than in the lateral direction, and the dimensions of the flock are increased and decreased as noise level and force constant respectively are raised.

3.2.1 Ordered regime

In Fig. 3.15, we plot the polarisation as function of η for various levels of γ.

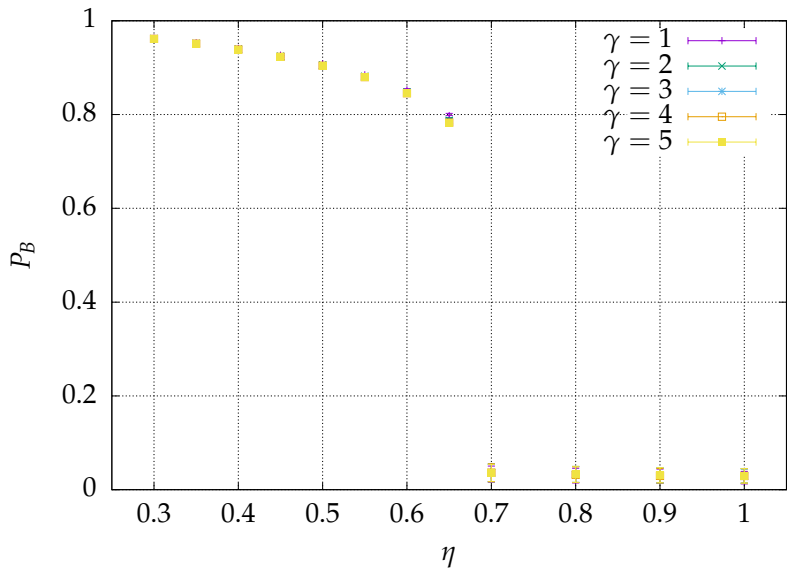

Figure 3.15: *Order parameter P_B as function of noise level η, for various force constants γ, using the local curvature force recipe.*

As can be expected, the behaviour is qualitatively the same as in the local curvature recipe and the periodic Vicsek model, with the same phase transition from an ordered state to a disordered state at $\eta_C \approx 0.66$. In Fig. 3.16, we plot the shapes of the convex hulls as function of force constant for various noise levels.

Version of May 31, 2017– Created May 31, 2017 - 17:35

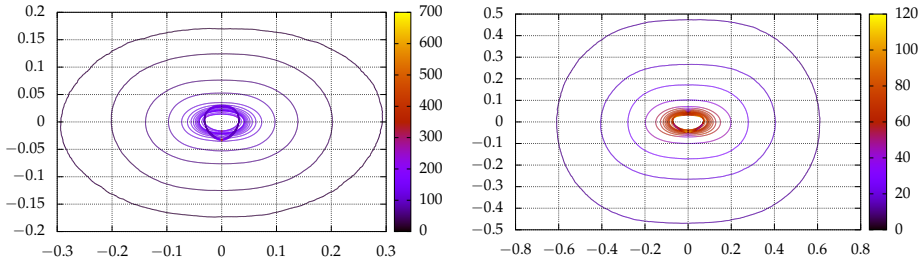

(a) $\eta = 0.10$ ***(b)*** $\eta = 0.20$

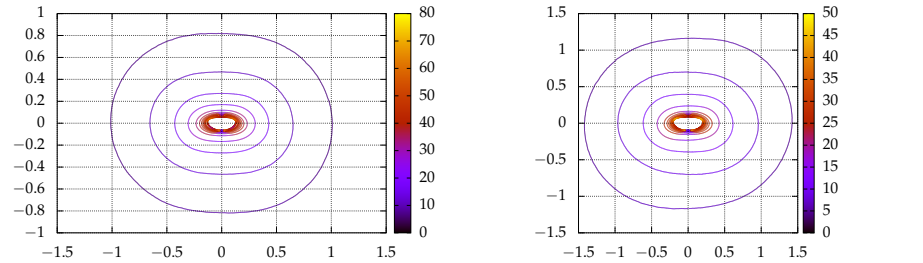

(c) $\eta = 0.30$ ***(d)*** $\eta = 0.40$

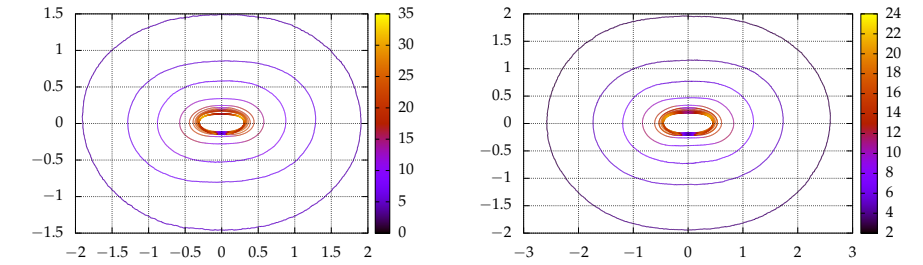

(e) $\eta = 0.50$ ***(f)*** $\eta = 0.60$

Figure 3.16: *Shape of the convex hull using the boid mean position force recipe for various noise levels and force constants between $\gamma = 0.1002$ and $\gamma = 631$, colour-coded to local hull density. The front of the hull is at the top.*

Again, the shape of the hull is widened in the direction transverse to the polarisation, for all values of η, much like in the local curvature force recipe. Where the behaviour starts to diverge, however, is in the finer detail of the shape of the convex hull and distribution of boids within the bulk: the hull approaches the shape of an ellipse for all η, and at low lev-

els of noise, the density of Boids on the hull and in the bulk is much more uniform than at comparable noise levels in the local curvature recipe. As the strength of this force recipe is proportional to the separation from the mean position of all boids, boids deflected near the front are influenced less by the hull, compared to the sides. This, coupled with the lack of response to the curvature, preclude the circulatory phenomena found in the local curvature force recipe.
Furthermore, for low noise ($\eta = 0.10$ and $\eta = 0.20$), a very high value of γ actually deforms the shape of the hull to such a degree that it is longer than it is wide. The cause of this is a combination of the low noise level giving way to a small convex hull (of order $\sim \ell$ in the direction of polarisation), and the high force constant pointing strongly into the direction of the mean position. The result is that boids at the front and sides of the hull are strongly displaced toward the mean position, overshooting the center as the bulk moves and reaching the back of the hull and displacing the mean position from the center of the hull to the back, where the force on the hull becomes much weaker due to its proximity to the mean position of Boids.
In Fig. 3.17, we plot the dependence of the surface area on η and γ, and find quantitatively different behaviour from the local curvature recipe.

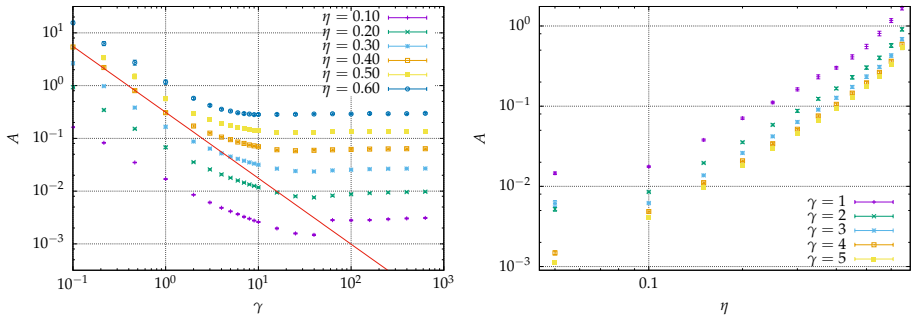

Figure 3.17: *Area as function of force constant in the flock mean force recipe. The slope in the lower γ regime corresponds to an exponent of -$\frac{5}{4}$, while the dependence on η is stronger than a power law.*

In the low γ regime, the surface area decreases with a power law of $-\frac{5}{4}$ before settling to a finite minimum, given by the noise. The deformation in the lower noise ranges is also reflected in a slight increase in this saturation value when the shape of the hull becomes elongated in the direction of motion. As a function of η, the surface area increases faster than a power law.
In Fig. 3.18, we plot the transport of Boids along the hull.

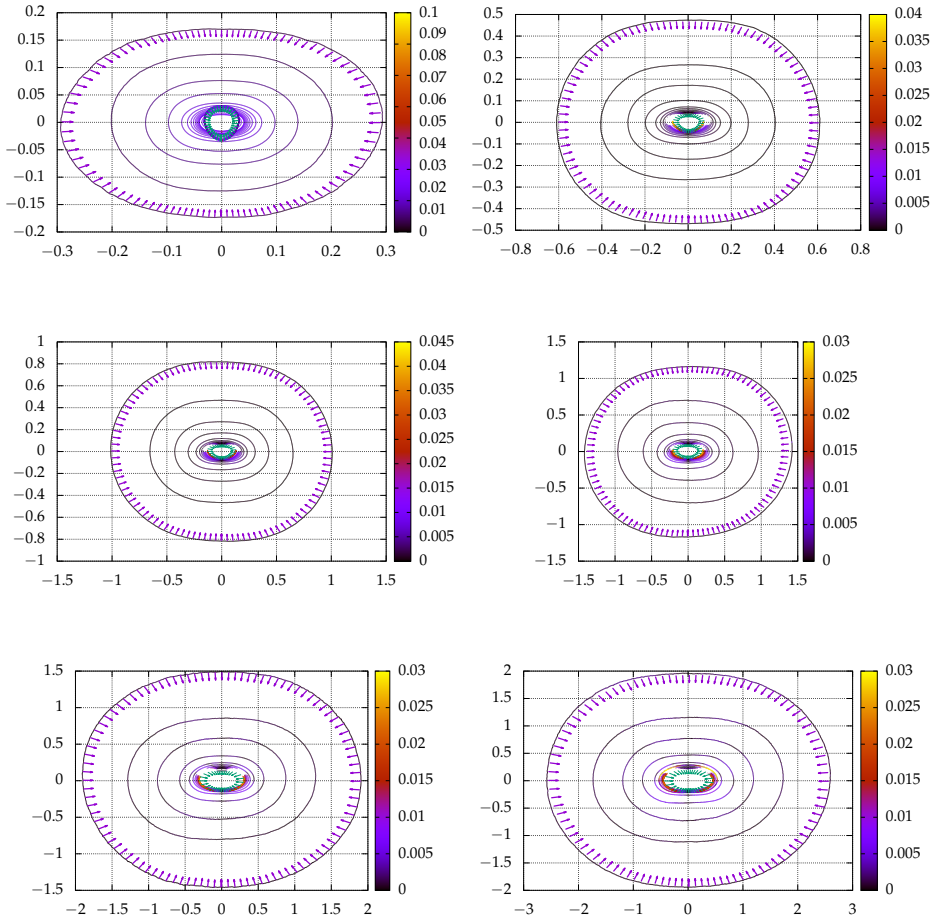

Figure 3.18: *Shape of the convex hull using the boid mean position force recipe for various noise levels and force constants, colour-coded to Boid transport. The layout is the same as in Fig. 3.16.*

At low force levels, transport on the hull is caused in spite of the force experienced by Boids, rather than because of it. Due to the low influence of the hull, high value of P_T and low density on the hull, boids can be deflected inward somewhat and still become part of the convex hull the next timestep at an angle very close to the previous position. For high values of γ, the transport on the hull happens due to boids overshooting their targeted mean position, resulting in relatively high speeds perpendicular to the centre of the hull. This does, however, prevent specific regions from being starting points for transport, as shown by the empty space at the sides of the front, which are too far away from other parts of the hull for Boids to be deflected toward: Boids on the convex hull in those regions

never landed on the convex hull a timestep afterward. In Fig. 3.19, we show the relative positions of Boids as they moved through the hull.

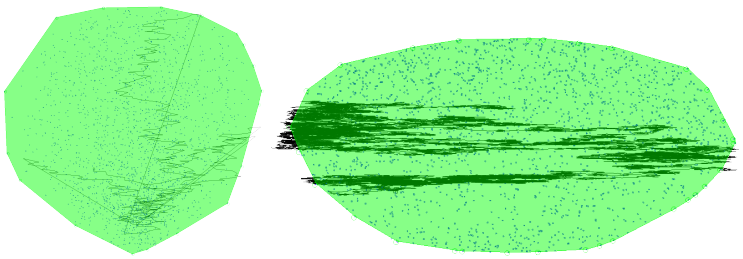

Figure 3.19: *Snapshots of the convex hull (polarisation pointing up) with $\eta = 0.10$, $\gamma = 100$ (left) and $\gamma = 1$ (right), with time traces of a boid as it moved relative to the hull.*

In the mean force recipe, no net precession occurs, much like the local curvature recipe. Its response to sudden changes in direction induced by high levels of noise, however, is much less dramatic: the hull adapts rapidly to changes in direction, and does not amplify the volatility of the direction of motion. In Fig. 3.20, we plot the dependence of the mean squared curvature on the noise level for various force constants.

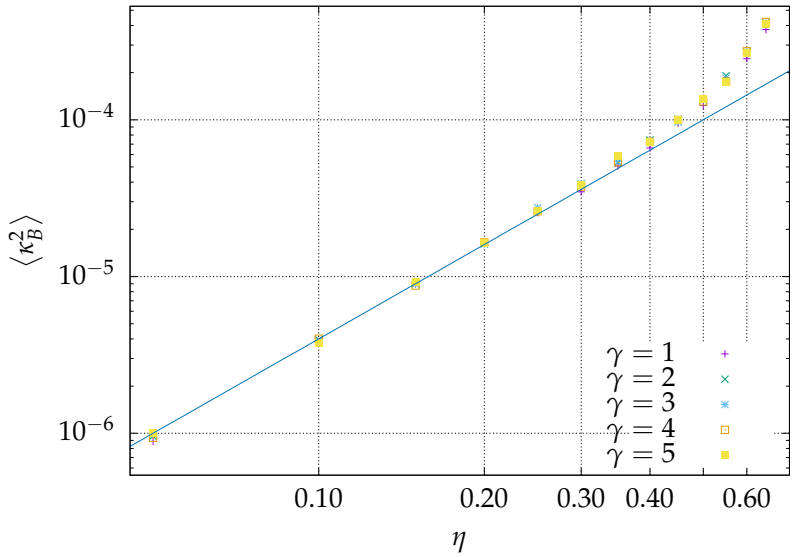

Figure 3.20: *Mean squared curvature as function of noise level in the flock mean force recipe.*

Here, the power law corresponds to an exponent of 2, as opposed to 2.5 in the local curvature.

In Fig.3.21, we plot the surface area A of the convex hull as function of the bulk's mean squared curvature $\langle \kappa_B^2 \rangle$.

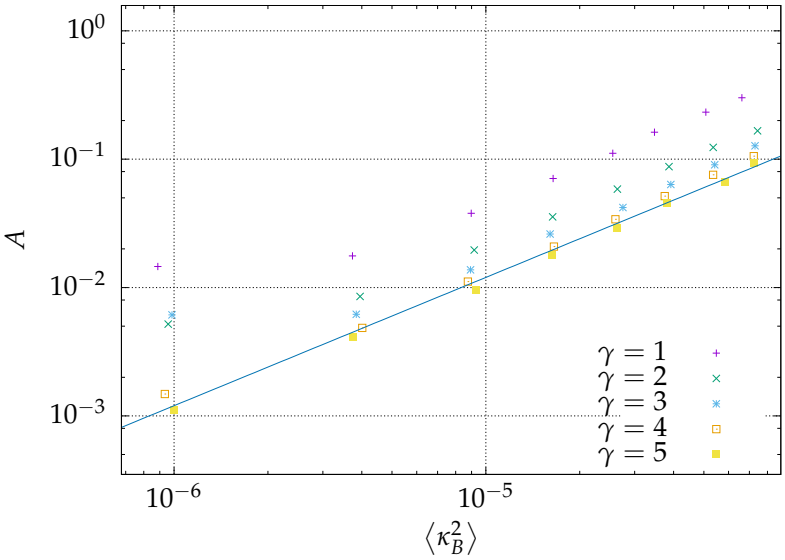

Figure 3.21: *Convex hull surface area as function of mean squared curvature in the flock mean force recipe.*

We find that the area grows linearly in the squared curvature, again a surprising result considering the lack of a power law relationship between A and η.

3.2.2 Disordered regime

Finally, we present the results of the behaviour of the local curvature recipe when the system is in a disordered state. We induced this disorder purely by raising the noise level above the critical value of $\eta_C \approx 0.66$, rather than lowering the force constant such that the density of the system becomes suitably low for global disorder while allowing local order. In this regime, the convex hull becomes roughly circular (as seen in Fig. 3.22) in shape, and no net motion occurs, up to some random walk behaviour.

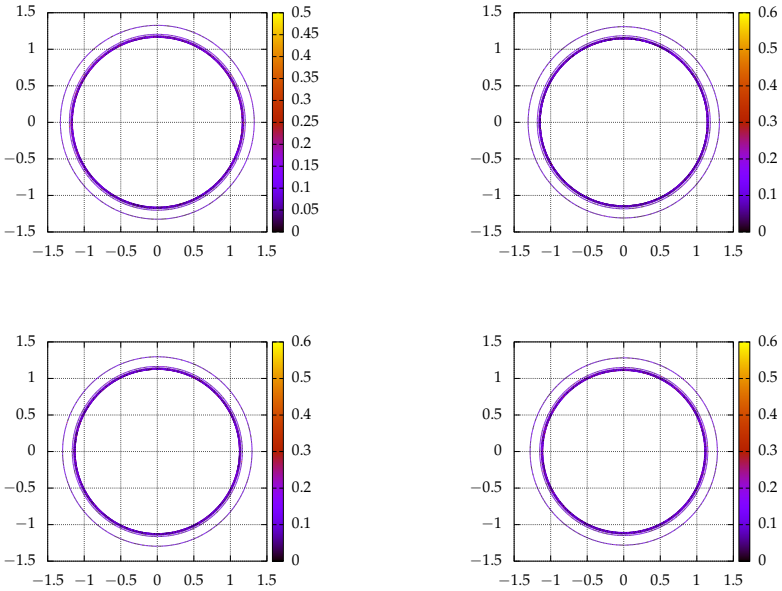

Figure 3.22: *Shape of the convex hull using the boid mean position force recipe for various noise levels above η_C and force constants between $\gamma = 0.3$ and $\gamma = 10$, colour-coded to local hull density* ***Top left****: $\eta = 0.7$,* ***top right****: $\eta = 0.8$,****bottom left****: $\eta = 0.9$,****bottom right****: $\eta = 1.0$.*

The surface area is quickly minimised to a finite value as γ is raised, which is only weakly dependent on η: in Fig. 3.23 we plot these dependencies.

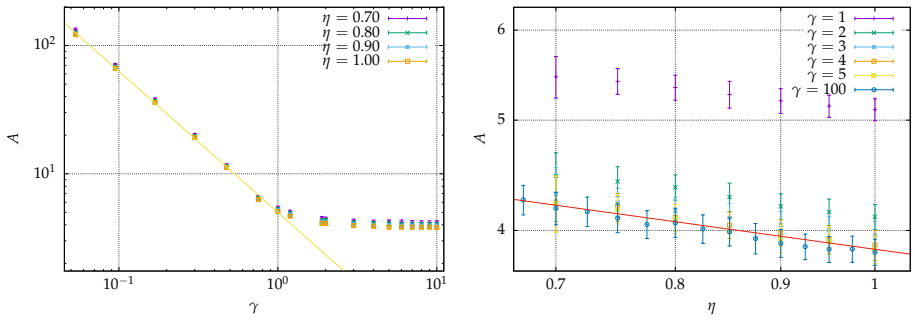

Figure 3.23: ***Left****: Surface area as function of force constant for various noise levels above η_C.* ***Right****: Surrface area as function of noise level above η_C for various force constants.*

We find $A \sim \eta^{-1/4}$, similar to the local curvature force recipe. Presumably, the same reason why we found such an unexpected exponent in the

local curvature force recipe, namely the lack of range in A, is why we find this value here. In the low values of γ, we find $A \sim \gamma^{-1.1}$.

3.2.3 Conclusion

The mean position force recipe presents a very simple, if nonlocal, implementation to prevent a flock from dissipating in the Vicsek model. We have found the quantitative behaviour to be quite different from the local curvature force recipe, and to remain stable in all regimes of η that would in a high-density periodic boundary version of the Vicsek model turn into an ordered state. In this force recipe, too we find some aberrant behaviour in the disordered state relating to the surface area A as function of noise level η. We expect probes with larger system sizes and force constants γ chosen such that the response of the flock is stronger to shed light on this behaviour.

3.3 Near Neighbour

We found the Near Neighbour force recipe to not actually compress the convex hull. Rather, boids on the hull spaced very close together will move toward one another, increasing the distance between their far neighbours. This in turn increases the force vector's length, eventually causing the force vector to point to the outside of the hull, ballooning the convex hull to arbitrary size. Because of this, we did not further pursue probes using this force recipe.

Version of May 31, 2017– Created May 31, 2017 - 17:35

3.4 Far Neighbour

We now move on to the recipe we investigated most, the Far-Neighbour force. This recipe is phenomenologically the most interesting, as it contains an additional symmetry breaking: a phase transition occurs, between a stationary state, where the distribution of boids and the shape of the convex hull are symmetric along the lateral axis, going through the center of the hull in the direction of the polarisation, and one whereby this symmetry is broken and the flock rotates.

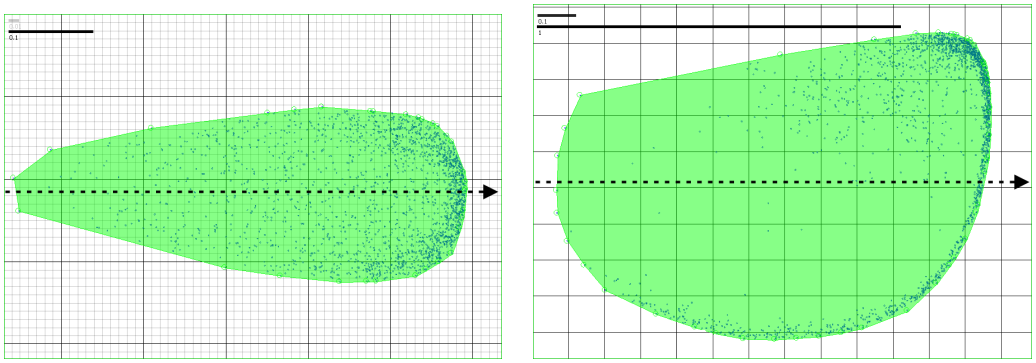

(a) The symmetric, straight path phase

(b) The asymmetric, rotating phase. In this case, the polarisation precesses clockwise.

Figure 3.24: *An instance of our model with identical parameters $\gamma = 2.5$, $\eta = 0.1$. While both phases are well in the ordered regime, the behaviour of the flock is different: the surface area of the stationary phase is smaller, as can be seen by the scale bars in the top left corner (bottom bar in the left image corresponds to top bar in the right image), and the distribution of boids, both in the bulk and on the hull varies wildly.*

Furthermore, in the ordered regime, the convex hull does not decrease in size as γ is raised. On the contrary: it increases, due to an elongation in the direction of motion. We have plotted the shape of the convex hull for various force constants while keeping the noise constant in Fig. 3.25.

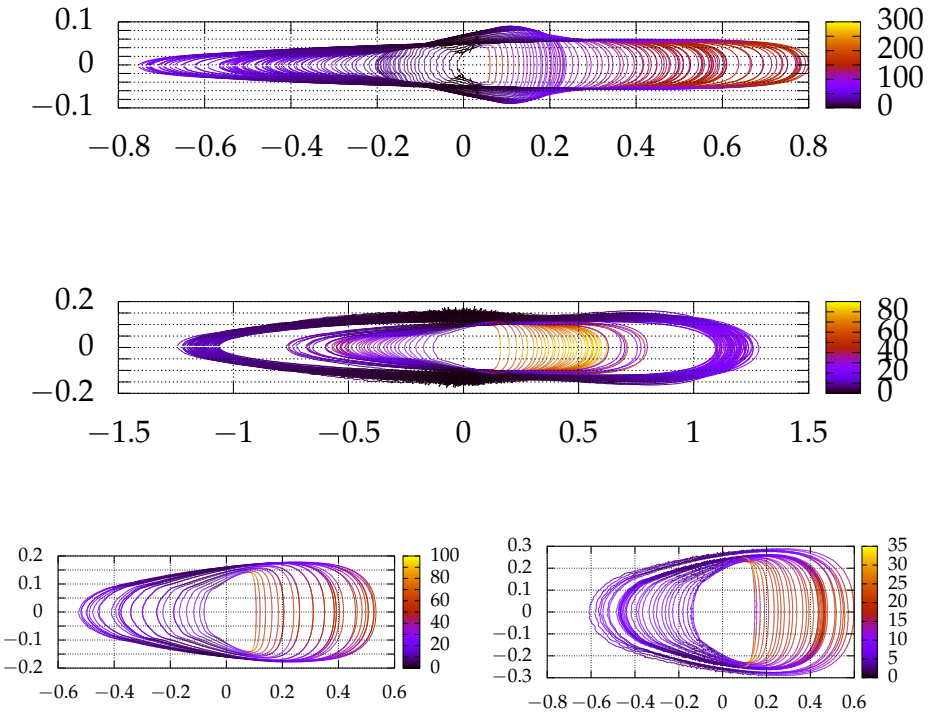

Figure 3.25: *Shape of the stationary phase convex hull for multiple noise levels and force constants, colour-coded to density. Starting with a low force constant, the hull is smallest. As the force constant is increased, the dimensions first grow equally, until reaching a maximum width. After this, the length of the hull keeps increasing to a finite value while the width decreases to another finite value, dependent on the noise level.* ***Top****:* $\eta = 0.05$*,* ***middle****:* $\eta = 0.10$*,* ***bottom left****:* $\eta = 0.15$*,* ***bottom right****:* $\eta = 0.20$*.*

For very low values of γ, the surface area does indeed decrease in size as the force is raised, as a vanishing force constant will allow the flock to balloon to an arbitrary size and cause a vanishing polarisation, even with very low levels of noise. We chose to restrict our probe to values of γ where disorder was caused only by a high noise level and found 2 regimes of change in the size of the convex hull. In the stationary state, the hull first increases in both directions roughly at the same rate, until the transverse dimension saturates to some value set by the noise level. At the same time, the lateral dimension asymptotically increases to some finite maximum, while the transverse dimension decreases again until reaching a nonvanishing minimum, again given by the noise level. This is summarised in Fig. 3.26

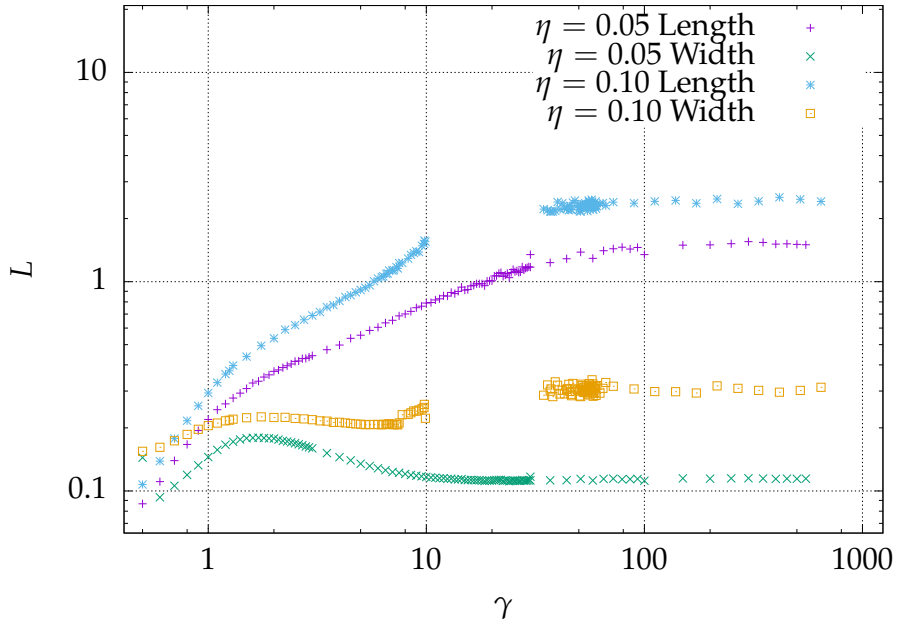

Figure 3.26: *Length and width of the stationary state for* $\eta = 0.05$ *and* $\eta = 0.10$ *for various force constants* γ.

A similar behaviour is found in the rotating phase, though its dependence on γ is of a smaller power. In Fig. 3.27, we present the shape of various rotating states.

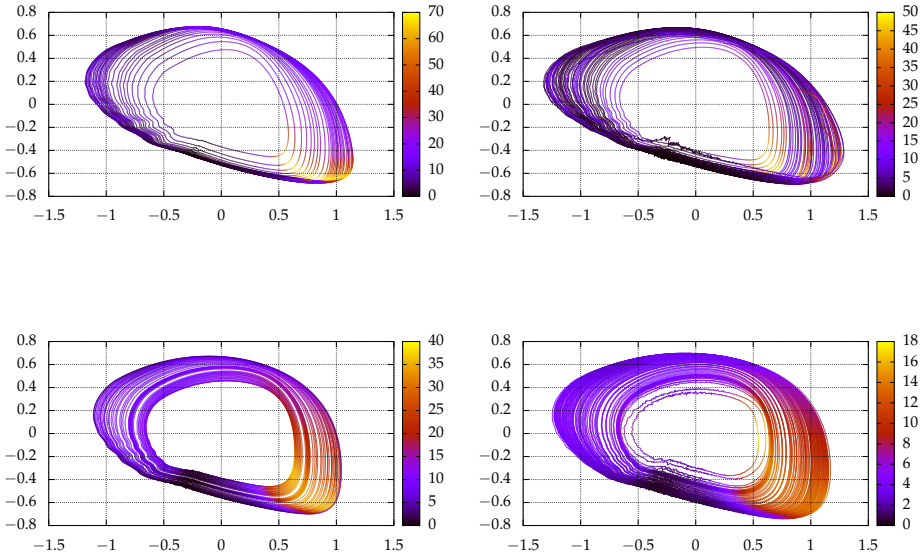

Figure 3.27: *Shape of the rotating phase convex hull for various force constants, colour-coded to density. Starting with a low force constant, the hull is smallest. As the force constant is increased, the dimensions first grow equally, until reaching a maximum width. After this, the length of the hull keeps increasing to a finite value while the width decreases to another finite value, dependent on the noise level.* ***Top left****:* $\eta = 0.05$*,* ***top right****:* $\eta = 0.10$*,* ***bottom left****:* $\eta = 0.15$*,* ***bottom right****:* $\eta = 0.20$*.*

In the rotating phase, the hull becomes wider in the long side than on the side in which the polarisation rotates. The density is highest at this point, both on the hull and in the bulk. As the noise level is raised, the entire hull becomes more rounded, though in the direction of motion, it remains larger. In Fig. 3.28, we plot the dimensions of the rotating phase as function of γ, for $\eta = 0.05$ and $\eta = 0.10$.

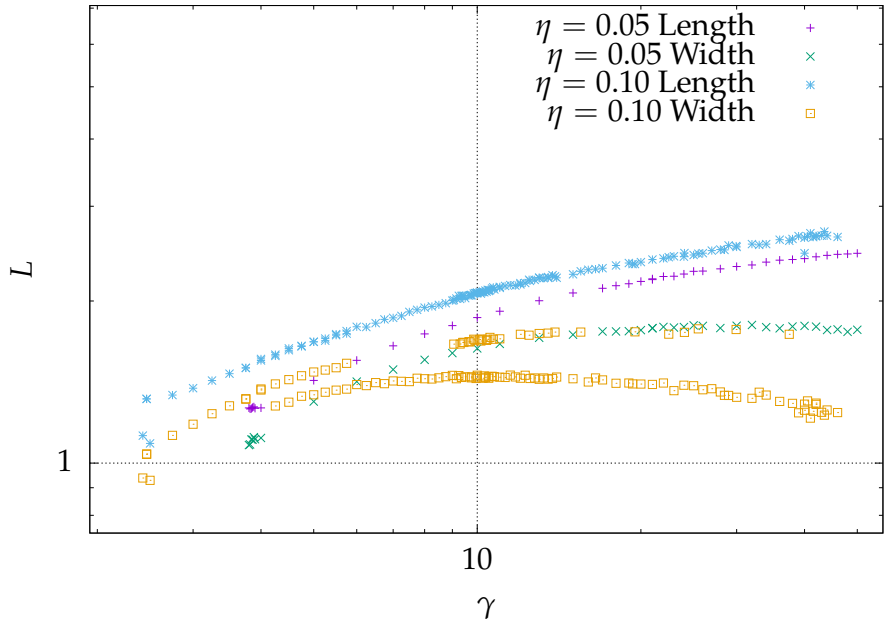

Figure 3.28: *Length and width of the rotating. state for* $\eta = 0.05$ *and* $\eta = 0.10$ *for various force constants* γ.

Concatenating these results, we present in Fig. 3.29 the surface area as function of force constant for various noise levels. Both the stationary and rotating phases are displayed, showing the clear jump in surface area at low η.

Version of May 31, 2017– Created May 31, 2017 - 17:35

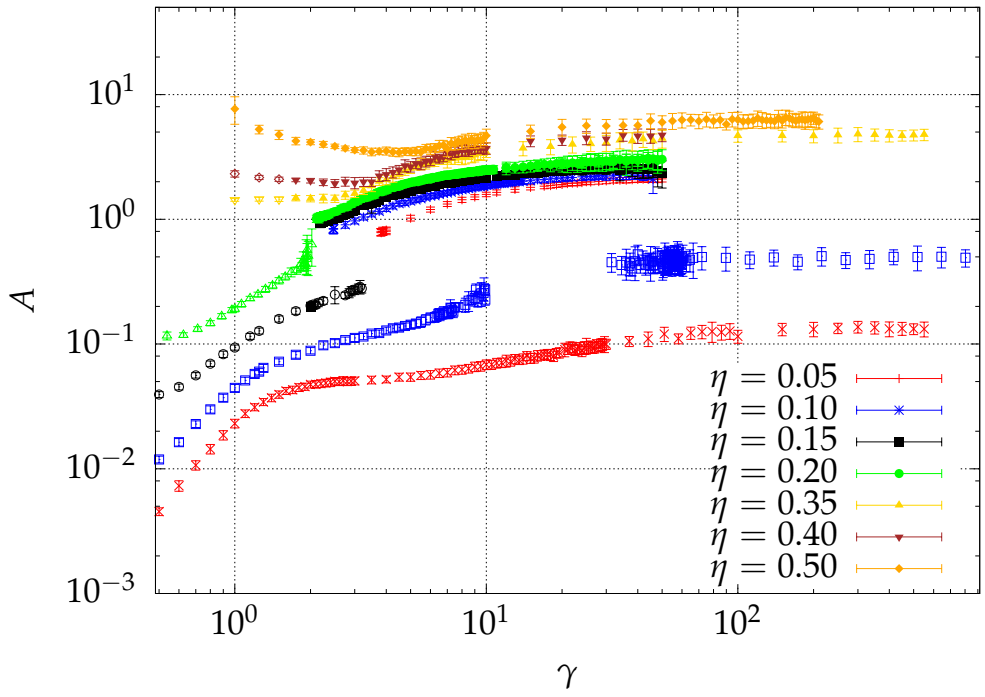

Figure 3.29: *Surface area A of the convex hull as function of force constant γ, for various noise levels η. Both the stationary and the rotating phases are plotted in the same colours, showing the clear jump in surface area. This gap is decreased as η increases, and for higher noise levels, it disappears entirely.*

As η increases, it becomes apparent that a region of exclusive existance of either phase starts to occur. While $\eta = 0.05$ and $\eta = 0.10$ still allow the flock to eventually collapse back to a stationary phase, as η is increased, this no longer occurs: raising the value of γ simply keeps the flock in a rotating phase of equal surface area. Furthermore, the phases become exclusively stable in specific regions until finally the distinction is blurred by a state that displays neither a definite direction nor a steady rotation.
In Fig. 3.30 and Fig. 3.31, we plot the transport of boids along the hull of the stationary state.

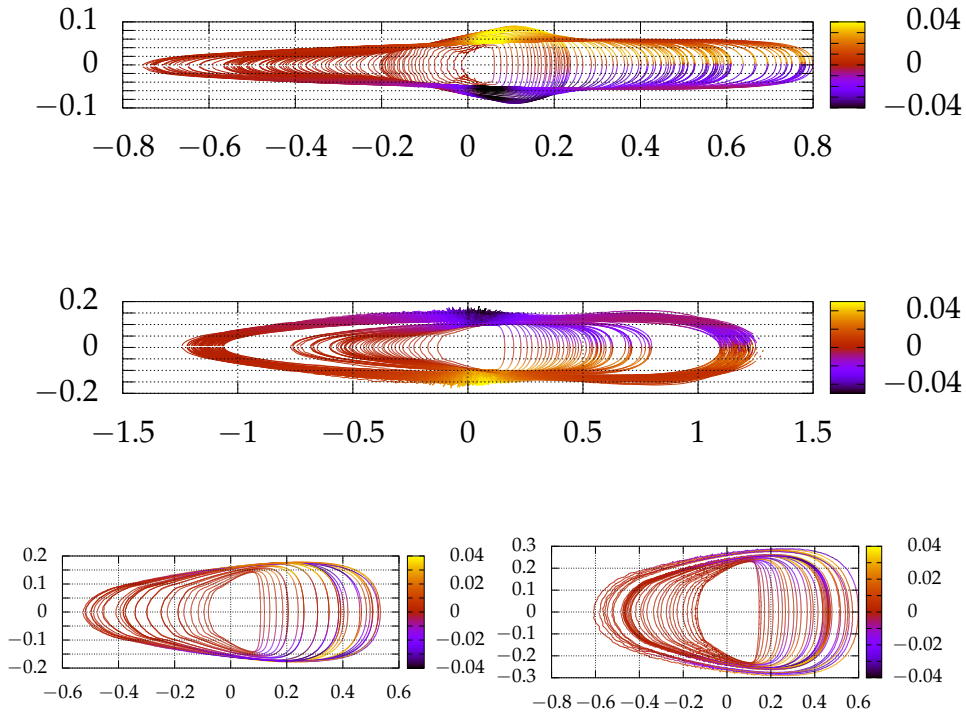

Figure 3.30: *Transport along the symmetric hull in the Far-Neighbour force recipe. The layout is the same as in Fig. 3.25*

In the stationary phase, symmetric along the sides, and seemingly takes place most intensely at a place of low density. Here, the force vector points toward a gradient in density, as the neighbouring boids become scarcer along the sides to the back. Eventually, boids reach a point of minimum density on the hull, and they are forced inward, to recombine with the bulk and restart the circulation. In Fig. 3.31, we plot the transport of the flock in a rotating phase.

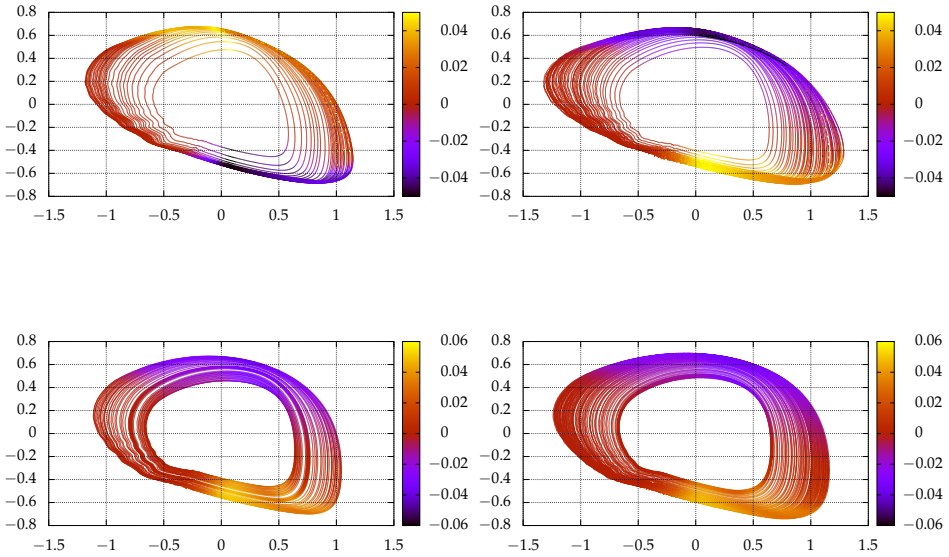

Figure 3.31: *Transport along the asymmetric hull in the Far-Neighbour force recipe. The layout is the same as in Fig. 3.27*

Similar to the stationary phase, transport occurs mostly from regions of high to low density. Furthermore, along the side that points outward during rotation, where the density is lower than on the other side of the hull, it is strongest. In Fig. 3.32, we plot simulated forces on the hull in both the stationary and rotating phases.

Version of May 31, 2017– Created May 31, 2017 - 17:35

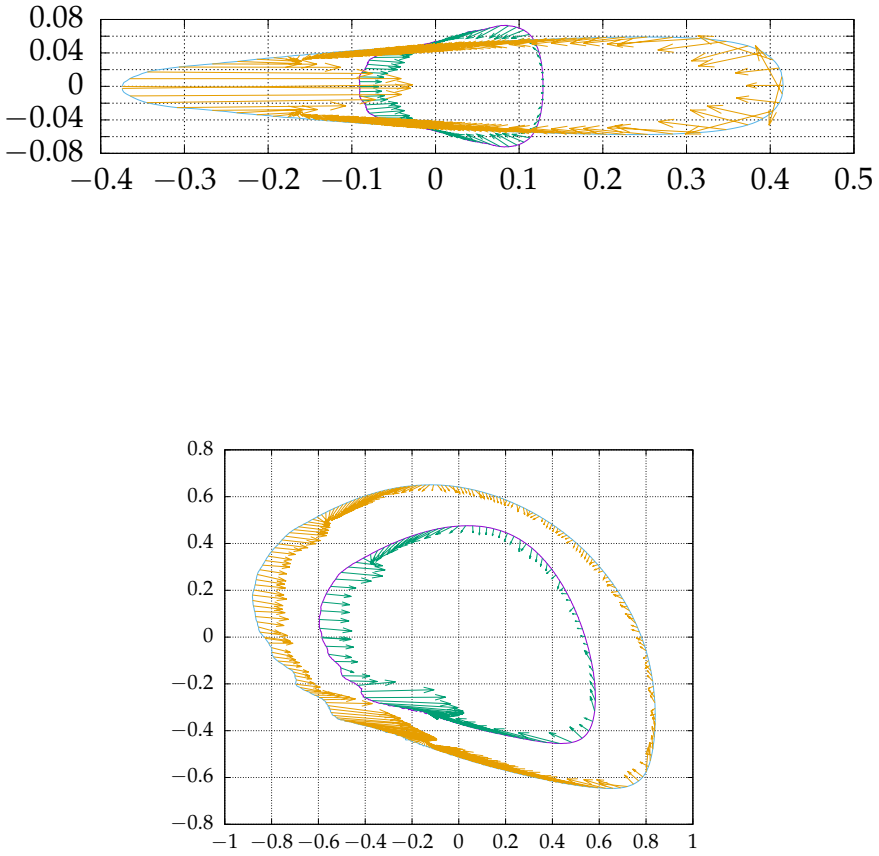

Figure 3.32: *Simulated forces on the convex hull in both the rotating and stationary phases.*

As we have seen in the results, in the stationary phase, transport is strongest along the sides of the front, where density experiences a gradient from high in the front to low on the sides. The force vector becomes strongly parallel to the hull, as neighbouring Boids are further away at the back than Boids closer to the front. Forces also appear to be strong in back, though these are in the direction of motion and in the direction of the geometric centre, and so this is not reflected in the transport found on the hull. Near the geometric centre, the forces on the hull start pointing back into the hull, as a result of the density reaching a minimum. This causes

a circulatory phenomenon: as Boids enter the bulk here, they are able to catch up with the hull, reaching the front again and restarting the process. In the rotating phase, a similar situation exists, though the circulatory effect is asymmetrical: boids on the side of the hull facing inward during rotating can be moved to the back of the hull, and move toward the side facing outward. From here, they are diffused into the bulk. While this happens, the bulk rotates, and these boids can migrate toward the inner side again. This is shown in Fig. 3.33

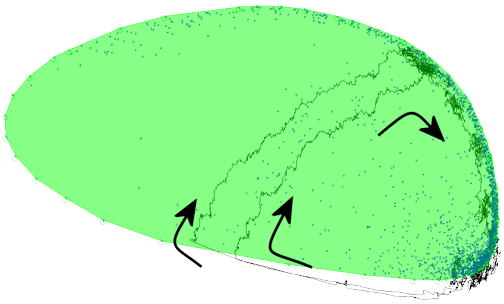

Figure 3.33: *Snapshot of the rotating phase, with a time trace of 6500 relative positions of a single boid as it moves through the flock.*

In the asymmetric phase, the polarisation precesses as the flock moves in a circular motion with a finite radius of curvature that is larger than the size of the hull, while the former causes the flock to move in a constant direction. The underlying cause behind this rotational state appears to be the interplay between the diffusive nature of the far-neighbour recipe trying to maintain a uniform density on the hull, and the bulk of the flock attempting to compensate for these changes in direction.
As the noise level is increased (beyond $\eta = 0.20$), this distinction is blurred, with the polarisation vector becoming variable purely due to noise itself. The asymmetry in the distribution of boids on the hull, however, remains. If we now focus on the regime of noise where this variability is minimal, some boundaries in the parameter space of γ, which themselves are dependent on η, can be identified:

- γ_{Min}, which is the minimum force constant required to keep the flock from ballooning to arbitrary size. Starting from here, the flock will assume the stationary state.
- $\gamma_{C_L^1}$, above which the rotating phase is also stable.
- $\gamma_{C_U^1}$, above which the stationary state is unstable. Using a stationary

Version of May 31, 2017– Created May 31, 2017 - 17:35

state thermalised to a slightly lower force constant as initial condition for simulations with $\gamma > \gamma_{C_U^1}$ will cause it to become rotational.

- $\gamma_{C_L^2}$, above which the stationary state again coexists with the rotational state.

- $\gamma_{C_U^2}$, above which the rotational state is no longer stable. Using a rotational state thermalised to a slightly lower force constant as initial condition for simulations with $\gamma > \gamma_{C_U^2}$ will cause it to become stationary.

The dependence of these values on η is not easily discerned: γ_{Min} simply increases as η is increased, which can be intuitively understood: as the noise of the system increases, greater influence from the hull must be exerted in order to keep the flock from ballooning up. However, C_L^1 decreases as γ becomes larger, allowing the existence of the rotational phase for lower γ at higher η. However, at very low noise, there is actually no region at which the stationary state is unstable: a region of coexistence exists, after which the stationary state becomes becomes the sole stable state again. At $\eta = 0.10$, a range of γ exists in which the rotating phase is preferable, but eventually the stationary state again becomes the only possible configuration to keep the flock in. As η is raised, this is no longer the case, and the rotating phase becomes preferable as $\gamma \to \infty$. At the same time, the phases become exclusive to their values of γ, until finally the noise is high enough that no clear rotation or steady movement occurs. The hull remains asymmetric for some range of η, however, until finally the flock is wider than it is long in the direction of polarisation, and the flock often changes its direction randomly.

This asymmetry is also reflected in the density of boids on the hull on both sides of the symmetry axis, as shown in Fig. 3.34.

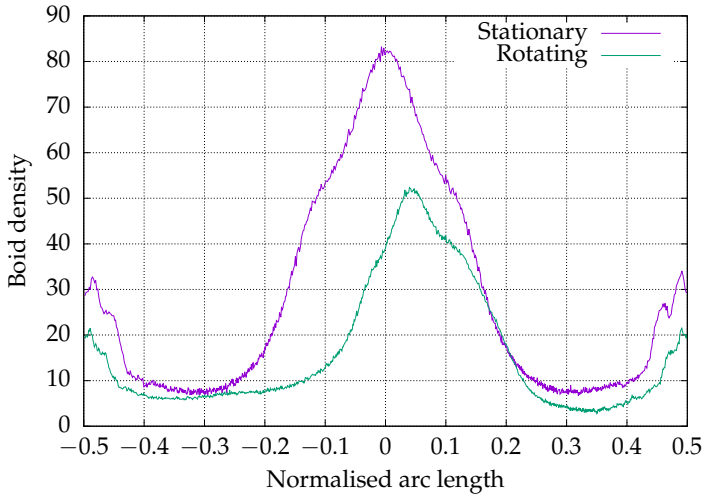

Figure 3.34: *Boid Density as function of position on the hull for equal values of noise and force constants ($\eta = 0.1$, $\gamma = 2.5$) in the Far-Neighbour force recipe.*

The speed at which the rotating phase precesses is dependent on both the force constant and the noise level: as a function of η, it decreases, until finally the asymmetric phase becomes highly variable in direction, with no clear rotation taking place. In the low noise levels, the rate of precession first climbs up to a maximum, and then monotonically decreases, while the higher noise levels leave no clear behaviour to be found, and the rate of precession appears to plateau. These results are summarised in Fig. 3.35.

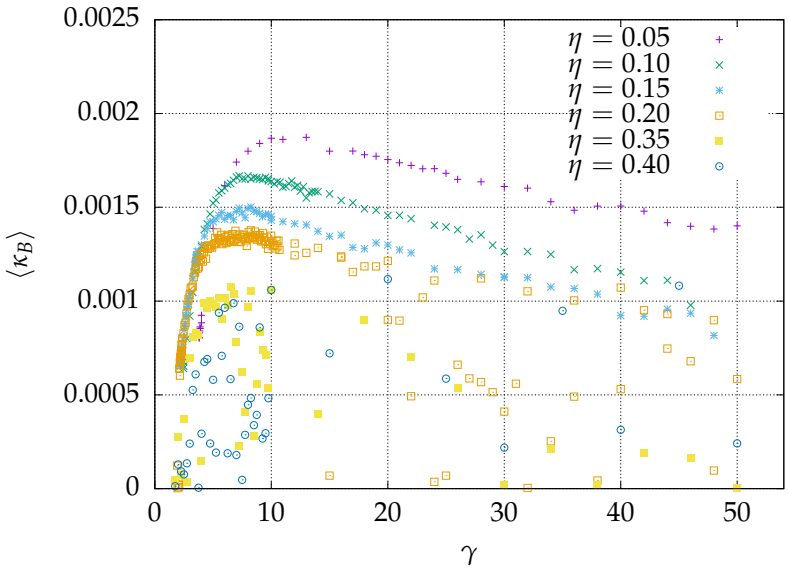

Figure 3.35: *Time-average of curvature κ_B in the rotating phase as function of force constant γ for various noise levels. As η is raised, the shape of the hull still stays similarly asymmetric, however its precession becomes less stable.*

This net rotation also leads to some different behaviour of the mean squared curvature compared to the irrotational state: in Fig. 3.36, we plot $\langle \kappa_B^2 \rangle$ as function of γ in both the stationary and the rotating states.

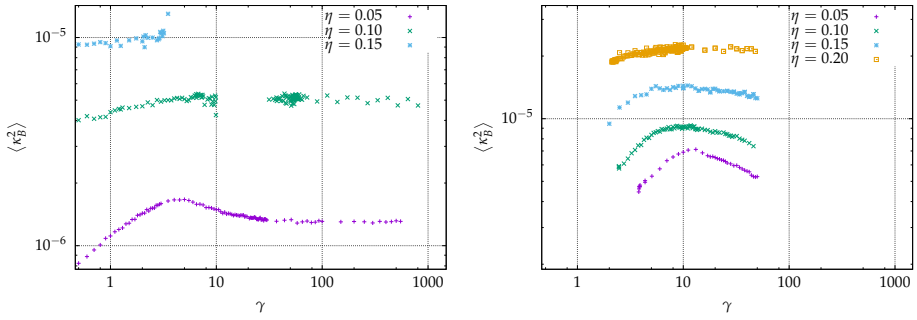

Figure 3.36: *Mean squared curvature of the far-neighbour force recipe as function of γ, in both the stationary (Left) and rotating (Right) phase.*

The peaks of $\langle \kappa_B^2 \rangle$ coincide at the peaks of $\langle \kappa_B \rangle$, and the lowest values of η have the lowest value of mean squared curvature, further showing the lower noise in the rotation. In the stationary phase, the peak in mean squared curvature coincides with the start of the coexistence with the rotating phase, which is surprising, considering the stability of either phase

Version of May 31, 2017– Created May 31, 2017 - 17:35

for a large range beyond this peak.

Disordered regime

In this section, we present results of the model while the system has a vanishing polarisation, i.e. $\eta > \eta_C$. With a suitably large number of boids and speed much lower than 1, the convex hull then takes the shape of a disk, the surface area of which is dependent on the noise level η, the force constant γ, the number of Boids N and the speed of the Boids v_0. In Fig. 3.37, we plot the dependence on v_0, and find a power law with exponent 2.11.

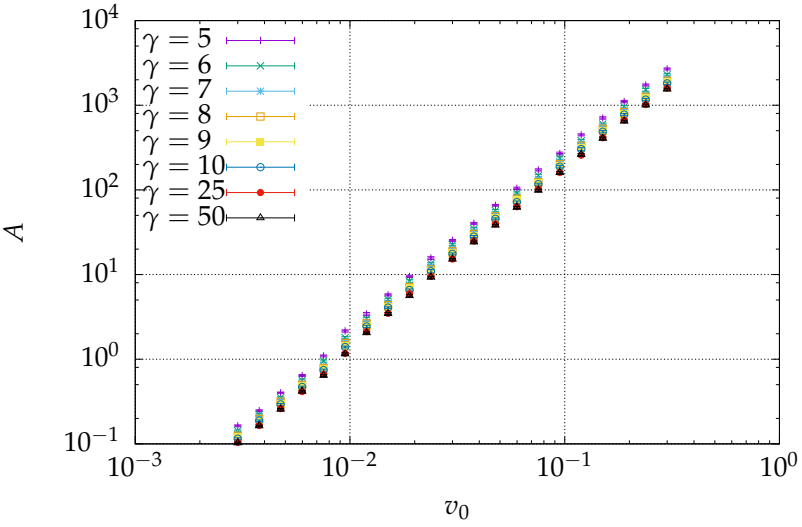

Figure 3.37: *Surface area A as function of boid speed v_0, with $\eta = 1.0$ The exponent of this power law is 2.11*

in Fig. 3.38 we plot the dependence of the surface area on γ, for various values of η above the critical theshold η_C.

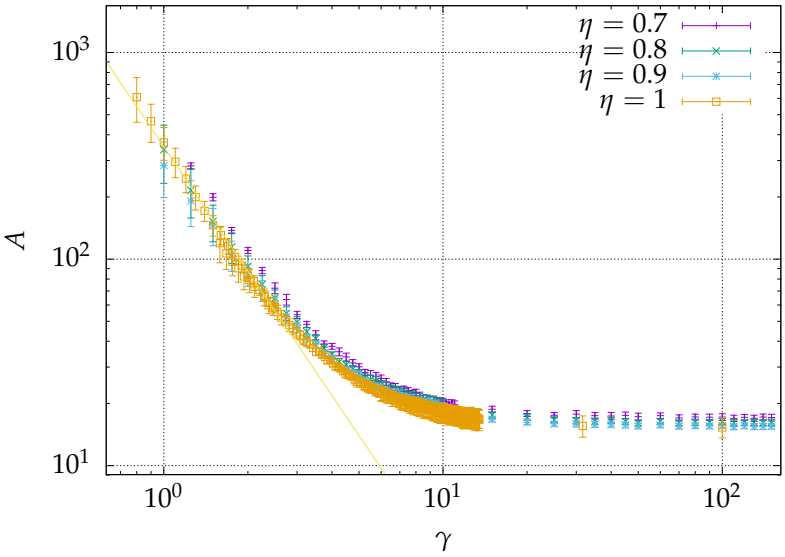

Figure 3.38: *Surface area A as function of force constant γ in the disordered regime, for different values of $\eta > \eta_C$. Before settling to a finite value, the surface area obeys a power law with $A \sim \gamma^{-2}$*

In contrast with the ordered phase, a higher force constant here does imply a smaller surface area. Furthermore, as the surface area decreases, it does so with a power law of γ^{-2}. In Fig. 3.39, we plot the surface area A as function of noise level η above η_C.

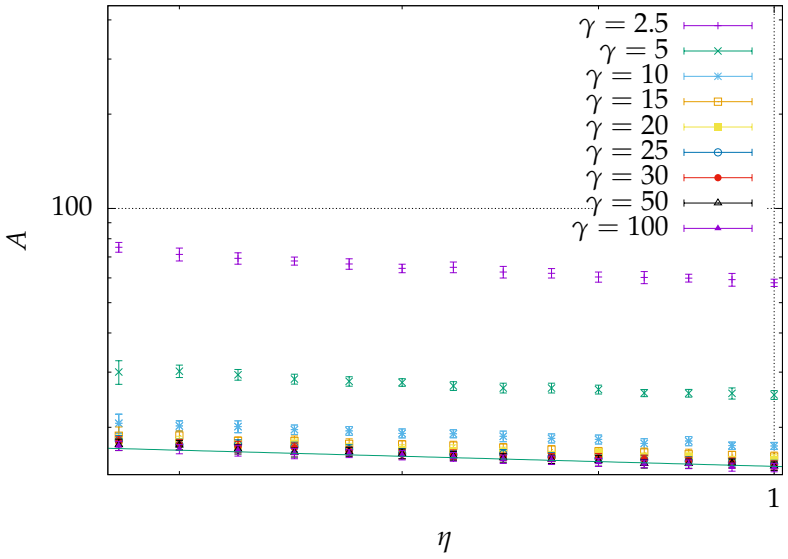

Figure 3.39: *Surface area A as function of noise level $\eta > \eta_C$ in the disordered regime, for different values of γ. The exponent of the power law is $-\frac{1}{3}$*

Again, the surface area decreases as η is raised. The power law here, too corresponds to an exponent of $-\frac{1}{3}$. Again, we expect this not to be accurate, as it does not fit into the idea that the pressure of the flock grows as the variance of the noise.

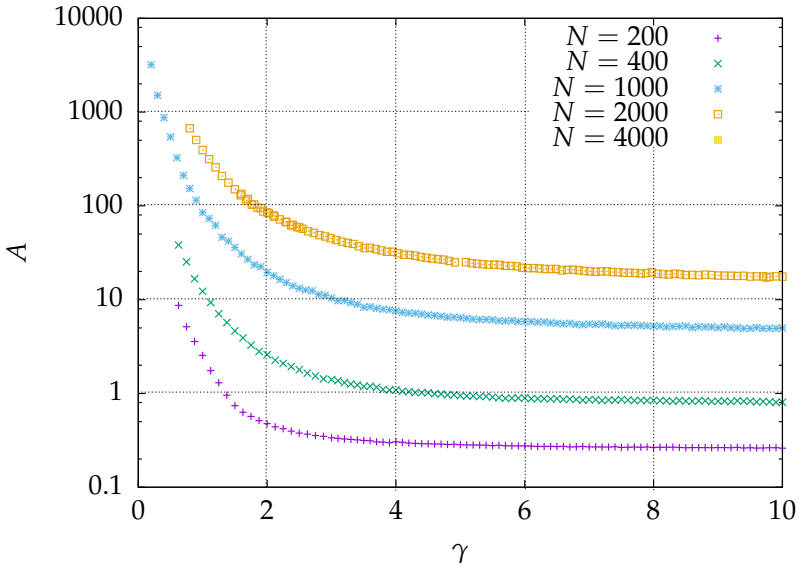

Figure 3.40: *Surface Area A as function of force constant γ with $\eta = 1.0$, for different numbers of boids N*

Conclusion

The Far-Neighbour force recipe presents an interesting new broken symmetry, presumably caused by the interplay between the diffusive mechanism of boids being deflected toward their farthest neighbours, attempting to maintain a uniform density on the hull, and the bulk's tendency to favour alignment. This interplay culminates in a rotation, the existence and dependence of which on η and γ is not trivial. We have shown the dependence of the surface area on the force constant and noise level, the transport of boids on the hull, in both the symmetric and the antisymmetric phases, as well as some simulated forces on both phases, further explaining the transport of Boids on the hull. Furthermore, in the disordered regime, the surface area of the convex hull again decreases as the noise is increased, with an exponent that does not seem to be dependent on the variance of the noise. Further investigations utilising a larger number of boids and a carefully chosen value of γ may offer insights into the behaviour of A.

References

[1] S. J. Decamp, G. S. Redner, A. Baskaran, M. F. Hagan, and Z. Dogic, *Orientational order of motile defects in active nematics*, Nature Materials **14**, 1110 (2015).

[2] M. Ballerini, N. Cabibbo, R. Candelier, A. Cavagna, E. Cisbani, I. Giardina, A. Orlandi, G. Parisi, A. Procaccini, M. Viale, and V. Zdravkovic, *An empirical study of large, naturally occurring starling flocks: a benchmark in collective animal behaviour*, ArXiv e-prints (2008).

[3] C. Becco, N. Vandewalle, J. Delcourt, and P. Poncin, *Experimental evidences of a structural and dynamical transition in fish school*, Physica A: Statistical Mechanics and its Applications **367**, 487 (2006).

[4] S. R. Sundaresan et al., *Social relationships and reproductive state influence leadership roles in movements of plains zebra, Equus burchellii.*, Animal Behaviour (2007).

[5] A. Czirók, E. Ben-Jacob, I. Cohen, and T. Vicsek, *Formation of complex bacterial colonies via self-generated vortices*, Phys. Rev. E **54**, 1791 (1996).

[6] B. Szabó, G. J. Szöllösi, B. Gönci, Z. Jurányi, D. Selmeczi, and T. Vicsek, *Phase transition in the collective migration of tissue cells: Experiment and model*, Phys. Rev. E **74**, 061908 (2006).

[7] I. D. Couzin and N. R. Franks, *Self-organized lane formation and optimized traffic flow in army ants*, Proceedings of the Royal Society of London B: Biological Sciences **270**, 139 (2003).

[8] V. Narayan, N. Menon, and S. Ramaswamy, *Nonequilibrium steady states in a vibrated-rod monolayer: tetratic, nematic, and smectic correlations*, Journal of Statistical Mechanics: Theory and Experiment **1**, 01005 (2006).

[9] C. W. Reynolds, *Flocks, Herds and Schools: A Distributed Behavioral Model*, SIGGRAPH Comput. Graph. **21**, 25 (1987).

[10] T. Vicsek, A. Czirók, E. Ben-Jacob, I. Cohen, and O. Shochet, *Novel Type of Phase Transition in a System of Self-Driven Particles*, Phys. Rev. Lett. **75**, 1226 (1995).

[11] G. Grégoire and H. Chaté, *Onset of Collective and Cohesive Motion*, Phys. Rev. Lett. **92**, 025702 (2004).

[12] A. P. Solon, H. Chaté, and J. Tailleur, *From Phase to Microphase Separation in Flocking Models: The Essential Role of Nonequilibrium Fluctuations*, Phys. Rev. Lett. **114**, 068101 (2015).

[13] J. Toner and Y. Tu, *Flocks, herds, and schools: A quantitative theory of flocking*, Physical review E **58**, 4828 (1998).

[14] J. Toner and Y. Tu, *Long-Range Order in a Two-Dimensional Dynamical XY Model: How Birds Fly Together*, Phys. Rev. Lett. **75**, 4326 (1995).

[15] H. Chaté, F. Ginelli, G. Grégoire, F. Peruani, and F. Raynaud, *Modeling collective motion: variations on the Vicsek model*, The European Physical Journal B **64**, 451 (2008).

[16] P. T. Nguyen, S.-H. Lee, and V. T. Ngo, *Effect of vision angle on the phase transition in flocking behavior of animal groups*, Phys. Rev. E **92**, 032716 (2015).

[17] D. J. G. Pearce and L. Giomi, *Linear response to leadership, effective temperature, and decision making in flocks*, Phys. Rev. E **94**, 022612 (2016).

[18] A. M. Andrew, *Another Efficient Algorithm for Convex Hulls in Two Dimensions*, Information Processing Letters **9**, 216 (1979).

[19] F. Ginelli, *The Physics of the Vicsek model*, European Physical Journal Special Topics **225** (2016).

Version of May 31, 2017– Created May 31, 2017 - 17:35